Journal of Theoretical Biology 352 (2014) 92–108

Contents lists available at ScienceDirect

Journal of Theoretical Biology

journal homepage: www.elsevier.com/locate/yjtbi

HTLV-I infection: A dynamic struggle between viral persistence and host immunity

Aaron G. Lim*, Philip K. Maini

Wolfson Centre for Mathematical Biology, Mathematical Institute, University of Oxford, Andrew Wiles Building, Radcliffe Observatory Quarter, Woodstock Road, Oxford OX2 6GG, UK

HIGHLIGHTS

- We develop a model for the host-virus dynamics of HTLV-I with target cell latency.
- A balance between proviral activation and latency aids viral persistence.
- Immune efficiency depends on rate of lysis and not on abundance of effector cells.
- Proviral activation may distinguish clinical status independent of proviral load.
- We hypothesise that crossing an activation threshold could increase risk of disease.

ARTICLE INFO

Article history:
Received 19 September 2013
Received in revised form
19 December 2013
Accepted 19 February 2014
Available online 28 February 2014

Keywords:
Mathematical modelling
Global stability
Proviral activation
Infected target cell latency
CTL response

ABSTRACT

Human T-lymphotropic virus type I (HTLV-I) causes chronic infection for which there is no cure or neutralising vaccine. HTLV-I has been clinically linked to the development of adult T-cell leukaemia/lymphoma (ATL), an aggressive blood cancer, and HAM/TSP, a progressive neurological and inflammatory disease. Infected individuals typically mount a large, persistently activated $CD8^+$ cytotoxic T-lymphocyte (CTL) response against HTLV-I-infected cells, but ultimately fail to effectively eliminate the virus. Moreover, the identification of determinants to disease manifestation has thus far been elusive.

A key issue in current HTLV-I research is to better understand the dynamic interaction between persistent infection by HTLV-I and virus-specific host immunity. Recent experimental hypotheses for the persistence of HTLV-I *in vivo* have led to the development of mathematical models illuminating the balance between proviral latency and activation in the target cell population. We investigate the role of a constantly changing anti-viral immune environment acting in response to the effects of infected T-cell activation and subsequent viral expression. The resulting model is a four-dimensional, non-linear system of ordinary differential equations that describes the dynamic interactions among viral expression, infected target cell activation, and the HTLV-I-specific CTL response. The global dynamics of the model is established through the construction of appropriate Lyapunov functions. Examining the particular roles of viral expression and host immunity during the chronic phase of HTLV-I infection offers important insights regarding the evolution of viral persistence and proposes a hypothesis for pathogenesis.

1. Introduction

Human T-lymphotropic virus type I (HTLV-I) is a persistent human retrovirus that infects between 10 and 25 million individuals world-wide (Bangham, 2000; Gallo, 2005; Goncalves et al., 2010; Mortreux et al., 2003; Proietti et al., 2005). It is the causative agent of two major, clinically independent diseases: an aggressive blood cancer called adult T-cell leukaemia/lymphoma (ATL), and a slowly progressive neurological and inflammatory disease, HAM/TSP. Despite significant advances over the past three decades, there still remain questions about the way in which HTLV-I-infected cells successfully evade a vigorous and chronically activated virus-specific host immune response mediated primarily by cytotoxic T-lymphocytes (CTLs) or the so-called 'killer T-cells' (Asquith and Bangham, 2007, 2008; Bangham et al., 2009, 1999). Furthermore, the precise mechanisms for the development of HTLV-I-associated diseases are unknown (Asquith and Bangham,

* Corresponding author.
E-mail addresses: aaron.lim@maths.ox.ac.uk (A.G. Lim), maini@maths.ox.ac.uk (P.K. Maini).

http://dx.doi.org/10.1016/j.jtbi.2014.02.022
0022-5193

2000; Bangham and Osame, 2005; Matsuoka and Green, 2009; Mosley et al., 2005). There is no cure or neutralising vaccine for HTLV-I, and neither is there an effective treatment available for HTLV-I-associated pathologies — infection is life-long (Bangham, 2000; Kubota et al., 2007; Mosley et al., 2005; Proietti et al., 2005).

A key unresolved issue in current HTLV-I research is how the virus is able to persist despite strong immune pressure and the implications of viral persistence on the outcome of infection. The focus of this paper is to develop a consistent theoretical framework that can help shed light on specific, biologically relevant questions that are of interest to experimentalists and theoretical immunologists trying to understand the complicated host–pathogen dynamics of chronic viral infections such as HTLV-I. We will investigate these questions using a mathematical modelling approach. Mathematical modelling can help us break apart the complex mechanisms of HTLV-I persistence and identify the underlying principles that govern successful viral propagation in the presence of host immunity. Understanding these interactions is a crucial step on the road to developing effective ways to disrupt the virus life-cycle and may help identify promising new treatment strategies to reduce the severity of HTLV-I infection and minimise the detriment due to the associated disease. More specifically, we formulate a mathematical model in order to elucidate the following:

(1) Since viral activation exposes infected cells to immune-mediated surveillance, why is HTLV-I not silent? In other words, what benefit does the HTLV-I provirus gain in becoming activated and expressing viral antigens?
(2) What determines the strength of the HTLV-I-specific CTL response, and why is infection life-long? That is, how can we evaluate the quality of the HTLV-I-specific CTL response, and why does host immunity fail to eradicate the virus?
(3) What characterises HTLV-I-linked pathology? Indeed, how can one determine the severity of viral detriment considering that the size of the proviral load is insufficient to classify clinical status? Can a mathematical modelling approach suggest an alternative, quantifiable measure to determine the outcome of the infection? If such a measure does exist, what implications might it have on the diagnosis, development, and treatment of HTLV-I-associated disease?

The organisation of this paper is as follows. In Section 2, we present our mathematical model, whose development has been strongly motivated by the immunological dynamics of HTLV-I infection *in vivo*, and motivate a biologically realistic range of parameter values which are adopted in numerical simulations. In Section 3, we discuss and establish the global qualitative behaviour present in the model. In Section 4, we distinguish two important measures of viral detriment which our modelling approach allows us to consider. Following this, we focus on the biological applications and outcomes of our mathematical model in Section 5, which we have subdivided into three themes corresponding to the three points raised above. Namely, in Section 5.1, we explore the effects of spontaneous viral expression that accompanies infected T-cell activation to understand why HTLV-I is not a completely silent infection. Then in Section 5.2, we consider factors that define an effective virus-specific cellular immune response and speculate why infection ultimately persists despite the presence of anti-viral host immunity. Next, we examine our mathematical model in the context of pathology in Section 5.3. Results from our investigations provide insights regarding HTLV-I-associated disease and suggest a novel hypothesis for pathogenesis. Lastly, in Section 6, we provide answers to the biological questions posed above by summarising the biological conclusions arising from examination of our mathematical model.

2. Methods

2.1. Mathematical model

Recently, Asquith and Bangham (2008) have proposed an experimental hypothesis for the infection and persistence of HTLV-I *in vivo* which motivated the formulation of a mathematical model by Li and Lim (2011) illustrating the balance between latency and activation in the target cell dynamics of the viral infection. In the model by Li and Lim (2011), the action of anti-viral host immunity was considered implicitly via fractions of newly infected cells that survive elimination. However, the pool of HTLV-I-specific immune effectors is highly dynamic and continuously changing in response to the virus population.

As cellular immunity is widely believed to be the most significant factor in determining the outcome of infection, we extend the model by Li and Lim (2011) to incorporate the two key features of HTLV-I infection *in vivo*: (i) viral latency, and (ii) the HTLV-I-specific CTL response. The separation of infected target cells into two distinct compartments, latently infected and actively infected, is crucial to understanding the persistence of HTLV-I in the midst of a chronically stimulated anti-viral host immune response.

The primary target cells of HTLV-I infection are $CD4^+$ helper T-cells, which we will initially separate into three different compartments. To model the explicit role of anti-viral cellular immunity, we also include an additional compartment of HTLV-I-specific $CD8^+$ cytotoxic T-lymphocytes (CTLs). In particular, we define

$x(t)$: density of healthy $CD4^+$ helper T-cells at time t,
$u(t)$: density of latently infected $CD4^+$ helper T-cells at time t,
$y(t)$: density of actively infected $CD4^+$ helper T-cells at time t,
$z(t)$: density of HTLV-I-specific $CD8^+$ CTLs at time t.

We consider a mathematical model of HTLV-I infection given by the following four-dimensional non-linear system of ordinary differential equations:

$$\begin{aligned}
\frac{dx}{dt} &= \overbrace{\lambda}^{\text{T-cell production}} - \overbrace{\beta xy}^{\text{infectious transmission}} - \overbrace{\mu_1 x}^{\text{natural death}} \\
\frac{du}{dt} &= \overbrace{\beta xy}^{\text{infectious transmission}} + \overbrace{ry}^{\text{mitotic transmission}} - \overbrace{(\tau+\mu_2)u}^{\text{spontaneous activation \& natural death}} \\
\frac{dy}{dt} &= \overbrace{\tau u}^{\text{spontaneous activation}} - \overbrace{\gamma yz}^{\text{CTL-mediated lysis}} - \overbrace{\mu_3 y}^{\text{natural death}} \\
\frac{dz}{dt} &= \overbrace{\nu y}^{\text{CTL proliferation}} - \overbrace{\mu_4 z.}^{\text{natural death}}
\end{aligned} \tag{1}$$

A schematic of the biological mechanism of HTLV-I infection *in vivo* upon which our model is based is shown for reference in Fig. 1.

Let us now motivate each term one by one. Naïve $CD4^+$ helper T-cells are produced in the bone marrow, then migrate to the thymus where they mature before being released into the peripheral blood. These mature $CD4^+$ helper T-cells are initially uninfected and we describe their rate of entry into the periphery by a constant λ. There are two routes of transmission for HTLV-I within the target cell population: horizontal or 'infectious', and vertical or 'mitotic'. Infectious transmission requires direct contact between an actively infected and a healthy target cell, and involves a restructuring of the cell cytoskeleton to create a tight junction known as a virological synapse, across which the viral genome is transported from the infected target cell to the uninfected one (Igakura et al., 2003; Shiraki et al., 2003). Upon infection, the newly infected target cell silences viral expression and becomes

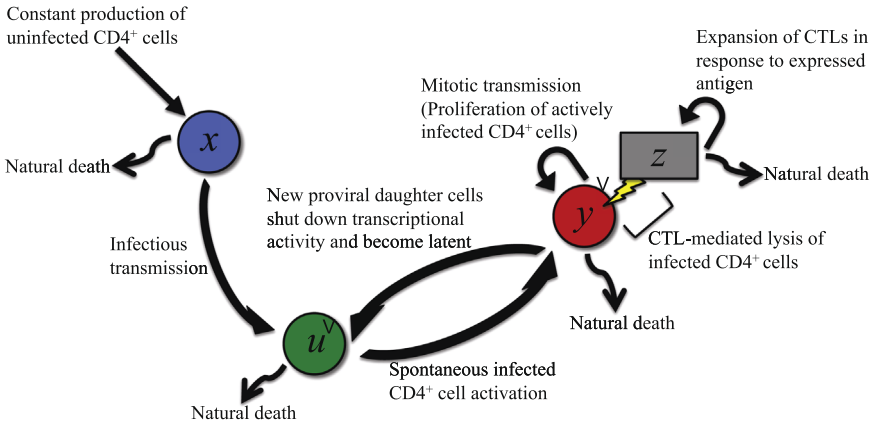

Fig. 1. A schematic representation of the biological mechanism of HTLV-I infection *in vivo* that motivates the formulation of model (1). Healthy $x(t)$, latently infected $u(t)$, and actively infected $y(t)$ target cells are represented by blue, green, and red circles, respectively, while HTLV-I-specific CTLs $z(t)$ are represented by grey rectangles. (For interpretation of the references to colour in this figure caption, the reader is referred to the web version of this paper.)

latently infected. The precise mechanisms behind the suppression of viral proteins are not yet understood (Asquith and Bangham, 2008). We describe the cell-to-cell virus transmission using a bilinear incidence term $\beta x(t)y(t)$, where β is the coefficient of infectious transmissibility. The mitotic route of transmission occurs when an actively infected target cell divides, creating two genetically identical daughter cells (Bangham, 2000). One way to represent the mitotic route of viral transmission is to assume that the proliferation of actively infected cells follows a logistic growth pattern given by a term $ry(t)(1-(x(t)+u(t)+y(t))/k)$, where r is the rate of rapid selective division, and k is the carrying capacity of $CD4^+$ helper T-cells. However, from studies of T-cell dynamics, the proliferation and removal rates of $CD4^+$ helper T-cells have been quantified (Asquith et al., 2007; Kirschner and Webb, 1996; Nelson et al., 2000), and suggest that the maximum proliferation rate is in general less than the rates due to natural death. Thus, it is plausible that even in the presence of rapid selective mitotic division, target cell populations do not exceed the total $CD4^+$ helper T-cell carrying capacity. We have investigated numerically the dynamics of the model using a full logistic growth term and observed no qualitative difference in the behaviour of trajectories (see Figs. B1 and B2 in Appendix B). Hence, with respect to our model we will assume that $x(t)+u(t)+y(t) \ll k$ for all $t \geq 0$, so that the proliferation of actively infected target cells follows an exponential growth profile. As a result, we choose to represent infected T-cell proliferation using an exponential growth term $ry(t)$ rather than a logistic growth term. As with infectious transmission, newly infected target cells via mitotic division immediately hide the expression of viral genes, thus entering the latently infected cell compartment and subsequently evading the immune system. At this point, we would like to remark that although mitosis is a process that occurs in all target cells, it has been experimentally shown that the rapid rate of infected target cell proliferation is significantly faster than normal homeostatic division (Asquith et al., 2007), but only during intermittent expression of the provirus (Asquith and Bangham, 2008; Richardson et al., 1997), coinciding in our model with the pool of actively infected target cells. Latently infected target cells do not express the provirus and proliferate at the same rate as normal, healthy $CD4^+$ helper T-cells. To avoid unnecessarily complicating the model equations, we do not consider the passive proliferation of healthy and latently infected target cells.

Latency allows the proviral cell to escape lysis by anti-HTLV-I CTLs, but hinders both the infectious and mitotic routes of viral transmission. Meanwhile, activation promotes viral transmission, but simultaneously exposes the proviral cell to immune surveillance (Asquith and Bangham, 2008). It is becoming increasingly clear that a dynamic balance between infected target cell latency and activation exists. Indeed, while the vast majority of proviral cells are latent at any given time Richardson et al. (1997), it has been observed experimentally that a small proportion of latently infected $CD4^+$ helper T-cells spontaneously express viral proteins and become actively infected (Asquith et al., 2000; Asquith and Bangham, 2008; Asquith et al., 2007). We represent the transition of a proviral cell from the latently infected state to the actively infected state by a term $\tau u(t)$, where τ is the rate of spontaneous infected T-cell activation or viral protein expression. In the activated state, proviral cells are subject to strong selection by HTLV-I-specific CTLs that recognise expressed HTLV-I antigens, such as epitopes on the immunodominant virus protein Tax and the minus-strand viral gene product HBZ (Gaudray et al., 2002; Goon et al., 2004). We model the elimination of actively infected target cells by virus-specific CTLs using a bilinear incidence term $\gamma y(t)z(t)$, where γ represents the rate of CTL-mediated lysis. The pool of CTLs is maintained by antigenic stimulation from virus-expressing activated proviral cells (Asquith et al., 2007; Bangham et al., 2009). The replenishment of these CTLs is described by the term $\nu y(t)$, where ν is the rate of CTL proliferation or turnover, also referred to as the CTL responsiveness (Nowak and Bangham, 1996; Wodarz et al., 2001).

Lastly, all T-cell populations under consideration, including $CD4^+$ helper T-cells and $CD8^+$ cytotoxic T-lymphocytes (CTLs), are removed from the system via natural cell death. We represent the removal of each cell type by a rate proportional to its density. Healthy, latently infected, and actively infected target cells die at respective rates μ_1, μ_2, and μ_3, and the removal rate of $CD8^+$ CTLs is μ_4.

All parameters are assumed to be positive. To close the model, we need to specify the initial conditions, and this is done in the next section.

2.2. Parameter values and numerical simulations

In this section, we discuss the parameter values that we use to simulate model (1), which have been estimated using both experimental and theoretical methods in studies of $CD4^+$ lymphocyte kinetics by Kirschner and Webb (1996) and Nelson et al. (2000). Asquith et al. (2005, 2007) have also quantified the *in vivo* kinetics of $CD4^+$ helper T-cells and $CD8^+$ CTLs in the context of persistent infection by HTLV-I in both asymptomatic carriers and in HAM/TSP patients. The production λ of healthy $CD4^+$ helper T-cells from the bone marrow falls in the range of 0–10 cells/mm^3/day (Kirschner and Webb, 1996). As infection by HTLV-I only causes minor detriment to T-cell functionality (Asquith and Bangham, 2007), it is expected that all three populations of target cells considered in our model display natural death rates similar to

Table 1
Table of biologically relevant dimensional initial conditions and parameter values. In general, median values have been selected. The ranges for each parameter can be found in the text.

Initial condition	Value (cells/mm^3)		Source
$x(0)$	$\sim$850		Bofill et al. (1992)
$u(0)$	0.1		Assumption on initial infection
$y(0)$	0.5		Assumption on initial infection
$z(0)$	0.1		Assumption on initial HTLV-I-specific CTL abundance
Dimensional parameter	**Value**	**Biological meaning**	**Source**
λ	10 cells/mm^3/day	Rate of production of target cells ($CD4^+$ helper T-cells)	Kirschner and Webb (1996)
β	0.001 mm^3/cell/day	Infectious transmissibility coefficient	Gómez-Acevedo and Li (2005), Gómez-Acevedo et al. (2010), Li and Lim (2011), Perelson (1989)
r	0.011 day^{-1}	Selective proliferation rate of actively infected cells	Asquith et al. (2007), Kirschner and Webb (1996)
τ	0.003 day^{-1}	Rate of spontaneous Tax expression	Asquith et al. (2007), Li and Lim (2011)
γ	0.029 day^{-1}	Rate of CTL-mediated lysis of actively infected cells	Asquith et al. (2005)
ν	0.036 day^{-1}	Proliferation rate of CTLs (or CTL responsiveness)	Asquith et al. (2007)
μ_1	0.012 day^{-1}	Natural death rate of healthy cells	Kirschner and Webb (1996), Nelson et al. (2000), Ribeiro et al. (2002)
μ_2	0.03 day^{-1}	Natural death rate of latently infected cells	Kirschner and Webb (1996), Nelson et al. (2000), Ribeiro et al. (2002)
μ_3	0.03 day^{-1}	Natural death rate of actively infected cells	Kirschner and Webb (1996), Nelson et al. (2000), Ribeiro et al. (2002)
μ_4	0.03 day^{-1}	Natural death rate of virus-specific CTLs	Ribeiro et al. (2002)

those of healthy target cells, with rates between 0.01 and 0.11 day^{-1} (Kirschner and Webb, 1996; Nelson et al., 2000; Ribeiro et al., 2002). Extracting from studies of HIV-1 infection (Ribeiro et al., 2002), it is assumed that activated $CD8^+$ CTLs die at similar rates in both uninfected and infected individuals, with the death rate lying between 0.03 and 0.05 day^{-1}. The rate of rapid Tax-driven selective mitosis r lies within the range 0.01–0.045 day^{-1} (Asquith et al., 2007; Kirschner and Webb, 1996), with higher rates of $CD4^+$ helper T-cell turnover usually associated with disease status, e.g. HAM/TSP.

We consider values for the coefficient of infectious transmissibility β to be on the order of 10^{-3} mm^3/cell/day, which is consistent with those used in recent mathematical models of HTLV-I infection (Gómez-Acevedo and Li, 2005; Gómez-Acevedo et al., 2010; Li and Lim, 2011). Asquith et al. (2007) have quantified the rate of expression τ of Tax in proviral cells to be between 0.0003 and 0.03 day^{-1}, and an intermediary value of 0.003 day^{-1} is chosen. The rate of lysis by anti-HTLV-I CTLs γ in asymptomatic carriers of the virus depends on each individual, and has been measured to be between 0.007 and 0.220 per $CD8^+$ cell per day with a median value of 0.029 day^{-1} (Asquith et al., 2005). Finally, the proliferation rate of HTLV-I-specific $CD8^+$ CTLs has been measured to be in the range 0.009–0.161 day^{-1} with a median value of 0.036 day^{-1} (Asquith et al., 2007). The biological meaning of the parameters, the primary sources for the parameter ranges, and the specific choices for the dimensional parameter values within the relevant ranges are summarised in Table 1.

Before we can solve model (1), we discuss a biologically reasonable initial state of the system at the onset of infection. In the absence of infection, the normal $CD4^+$ helper T-cell count averages 850 cells/mm^3 of peripheral blood, although it is known that there is a wide variance between individuals, with healthy values in adolescents and adults ranging from 500 cells/mm^3 to 1200 cells/mm^3 (Bofill et al., 1992).[1]

We assume that the individual is initially healthy, and that the start of infection occurs after the introduction of a small dose of infected cells, say on the order of 10^{-1} cells/mm^3. Next, it is known that CTLs of a diverse range of specificities are continuously being produced. The average level of $CD8^+$ cytotoxic T-lymphocytes in a normal, healthy individual is roughly 550 cells/mm^3 of peripheral blood (Bofill et al., 1992). We will assume that at the start of infection, the number of circulating $CD8^+$ CTLs in an individual that can recognise HTLV-I epitopes is on the order of 10^{-1} cells/mm^3. Here we remark that although the magnitude of the initial level of viraemia is small relative to the size of the target cell pool, these values, measured in units of cells per mm^3 of peripheral blood, are assumed to be homogeneous throughout the entire body of an individual, whose blood volume is several orders of magnitude higher ($\sim$5.5 L of blood for an average human weighing roughly 70 kg). Thus, stochastic effects are negligible and we are justified in adopting a deterministic modelling approach.

To gain some insight as to how we will approach the mathematical analysis of model (1), we use these biologically motivated initial conditions and parameter values (summarised in Table 1), and run preliminary numerical simulations of the model. Using the built-in differential equation solver in Mathematica (version 9.0.1.0), we solve model (1) numerically and plot the solution as in Fig. 2. The NDSolve command in Mathematica automatically selects a numerical algorithm to optimally solve the designated system of ordinary differential equations, and includes both explicit and implicit methods such as Euler, Adams, and Runge–Kutta of arbitrary order. Fig. 2(a) shows all four cell populations and highlights their relative abundances. As the magnitudes of the terms in the u, y, z-equations are much smaller than those of the x-equation, we take a closer look at their behaviours by magnifying the vertical axis, roughly 30 times in Fig. 2(b) and 600 times in Fig. 2(c). We observe that after some time, the solution appears to settle at a positive equilibrium which may be reached by damped oscillations. In the following section of the paper, we will examine the underlying dynamical behaviour of model (1) in more detail.

3. Global qualitative behaviour

Undoubtedly, one of the greatest advantages to modelling the HTLV-I system using a mathematical rather than a verbal approach is that we can make use of mathematical techniques to rigorously

[1] For reference, Acquired Immune Deficiency Syndrome (AIDS) caused by the human immunodeficiency virus (HIV) is characterised by a $CD4^+$ helper T-cell count below 200 cells/mm^3.

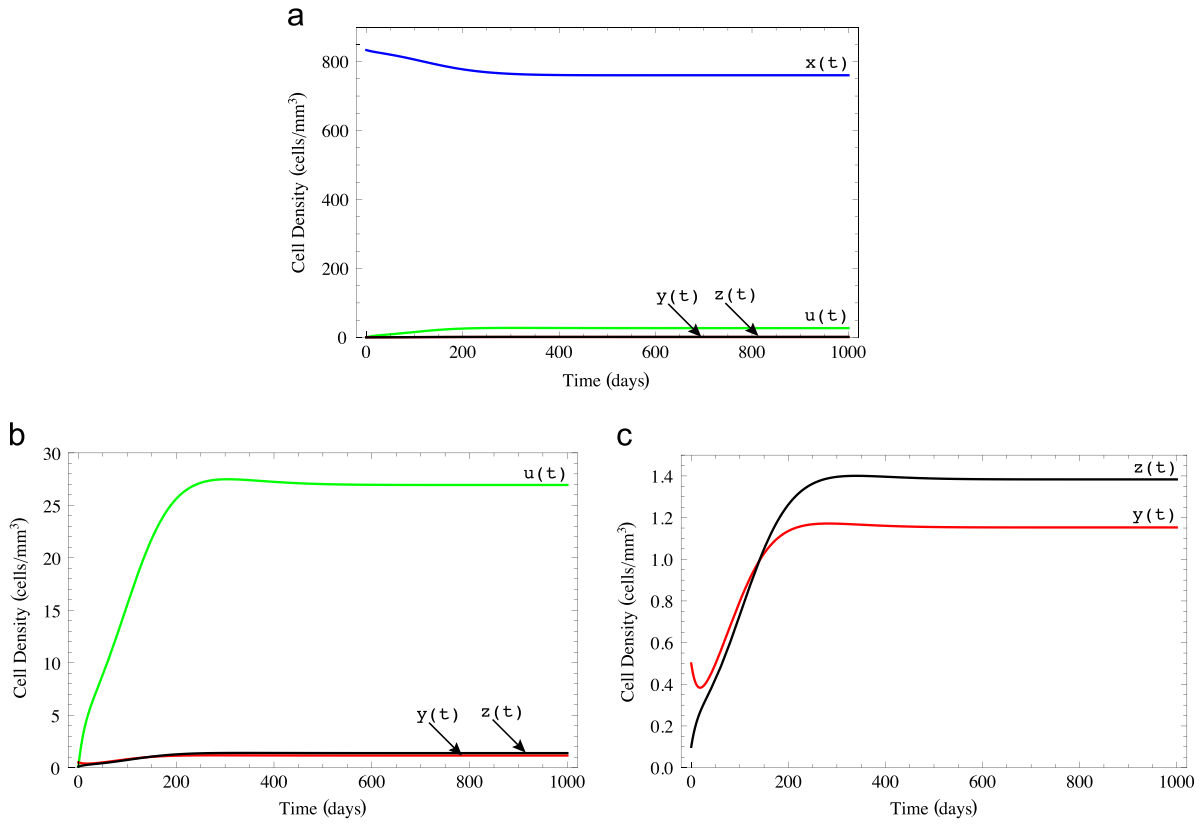

Fig. 2. Numerical simulation of the solution of model (1) with initial conditions and parameter values as in Table 1. The level of healthy $x(t)$, latently infected $u(t)$, and actively infected $y(t)$ target cells are shown in blue, green, and red, respectively, and the level of HTLV-I-specific CTLs $z(t)$ is shown in black. (a) The full dimensional range showing all cell populations and highlighting their relative abundances. (b)–(c) A closer examination of the behaviour of $u(t)$, $y(t)$, and $z(t)$ in model (1). (For interpretation of the references to colour in this figure caption, the reader is referred to the web version of this paper.)

and unambiguously characterise model behaviour, allowing for a systematic way to draw inferences from the model results. A well-defined mathematical model also allows us to identify specific processes that can lead to experimental designs to test the validity of the model representation we have chosen and determine its applicability to the biological system under study.

The purpose of this section is to provide a complete mathematical description of the global qualitative behaviour of all possible solutions of model (1). Establishing the global dynamics of our mathematical model means that we have a complete understanding of the qualitative behaviour of solutions of the model. This puts us in a position where we can fully explore the model without having to worry about the occurrence of unexpected phenomena, and allows us to draw robust conclusions from further investigations of the model in the remainder of this paper.

The first step in the mathematical analysis of model (1) is to determine a bounding region for the T-cell populations to ensure that our model is biologically reasonable. In particular, T-cell populations should neither become negative nor should they become unbounded. Our first result, Theorem 3.1, formalises such a notion. For the proof, the reader is referred to A.1. Denote by $\mathbb{R}^4_+$ the closed positive orthant of $\mathbb{R}^4$.

It can be seen from the model equations that for any set of non-negative initial conditions, $x,u,y,z \geq 0$ for all $t \geq 0$. Let $\mu = \min\{\mu_1,\mu_2,\mu_3\}$, and consider the closed, bounded region:

$$\Gamma := \left\{ (x,u,y,z) \in \mathbb{R}^4_+ : x \leq \frac{\lambda}{\mu_1}, x+u+y \leq \frac{\lambda}{\mu - r}, z \leq \frac{\lambda\nu}{\mu_4(\mu-r)} \right\}.$$

Theorem 3.1. *Assuming that $r<\mu$, the set Γ is positively invariant with respect to model (1). All solutions are bounded for $t \geq 0$ and eventually enter Γ.*

The assumption that $r<\mu$ corresponds to experimental evidence indicating that the proliferation rate of $CD4^+$ helper T-cells is generally lower than the rate of removal due to natural death (Asquith et al., 2007; Kirschner and Webb, 1996; Nelson et al., 2000), Therefore, Theorem 3.1 defines the set Γ as a biologically feasible region on which the model dynamics may be analysed.

The global behaviour of model (1) depends crucially on a key parameter, the *basic reproduction number for viral infection*, defined as

$$R_0 = \frac{\tau}{\mu_3(\tau+\mu_2)}(\beta x_H + r) \quad \text{where } x_H = \frac{\lambda}{\mu_1}. \tag{2}$$

Biologically, R_0 represents the average number of secondary infected cells produced from a single actively infected cell over its lifetime. The expression for R_0 derived from model (1) displays a similar form to the one determined in the model by Li and Lim (2011).

The following theorem summarises our main mathematical result and establishes R_0 as a sharp threshold that characterises the global dynamics of model (1) in $\overline{\Gamma}$. We refer the reader to Appendix A for a rigorous mathematical proof of the result, which has been separated into three parts to facilitate the ease of understanding. Appendix A.2 deals with the existence and uniqueness of equilibria, while Appendices A.3 and A.4, respectively, demonstrate the stability properties of the infection-free and chronic infection steady states, whenever they exist. The global dynamical behaviour of model (1) has been established using the direct method of Lyapunov, which has been successfully employed in proving the global stability of equilibria in population models from epidemiology (Kalajdzievska and Li, 2011; Korobeinikov and Wake, 2002) and immunology (Gómez-Acevedo et al., 2010; Korobeinikov, 2004).

Theorem 3.2 (*Global dynamics*).

(1) *The infection-free equilibrium* P_0 *always exists. Moreover, if* $0 < R_0 < 1$, *then* P_0 *is the only equilibrium in* $\overline{\Gamma}$ *and it is globally asymptotically stable in* $\overline{\Gamma}$.
(2) *If* $R_0 > 1$, *then the infection-free equilibrium* P_0 *is unstable. In addition, a unique chronic infection equilibrium* P^* *exists in* $\dot{\Gamma}$ *and it is globally asymptotically stable in* $\dot{\Gamma}$.

4. Measures of viral burden

One of the most important tasks faced by clinicians after identifying an HTLV-I seropositive individual is to evaluate the severity of the infection. How much damage has the virus caused to the host? Is the infected individual asymptomatic or are there signs of chronic or malignant disease? For the former, is the individual at risk of developing symptoms? For the latter, how far and how fast has the disease progressed? The degree of detriment caused by the virus is termed the *viral burden*.

The most common measure of viral burden in the host is the proviral load, and it is given by the proportion of all target cells in the peripheral blood that carry a provirus, regardless of their state of activation (Asquith et al., 2005; Asquith and Bangham, 2008). With the advance of current experimental techniques, such a measure, which simply reports the magnitude of the virus infection, is relatively easy to obtain from host sera and is frequently reported in experimental data as a percentage of all peripheral blood mononuclear cells (PBMCs) (Asquith et al., 2005). In terms of our mathematical model, we define the proviral load at equilibrium as the infected fraction of all $CD4^+$ helper T-cells:

$$v^* = \frac{u^* + y^*}{x^* + u^* + y^*}. \tag{3}$$

A defining characteristic of our mathematical modelling approach to HTLV-I infection is the separation of proviral cells into two distinct compartments based on infected target cell latency or activation. This allows us to consider how the two populations of proviral cells coexist and how they persist as the infection propagates back and forth through the latent and activated states. In our model, the total number of infected target cells, both latent and active, at equilibrium is given by the expression $(u^* + y^*)$. Thus, we can examine and define a second measure of viral burden to be the proportion of proviral cells that are activated, which is represented by the ratio:

$$\frac{y^*}{u^* + y^*}. \tag{4}$$

5. Results and discussion

5.1. Exploring spontaneous viral expression: why is HTLV-I not silent?

In HTLV-I infection, the vast majority of proviral cells do not express viral proteins at any given time, an observation that lends support to the traditional viewpoint that HTLV-I is largely inactive (Asquith and Bangham, 2008; Asquith et al., 2007). Nevertheless, it has been shown that most HTLV-I seropositive individuals, regardless of clinical status, mount a vigorous virus-specific cellular immune response, suggesting continuous stimulation by expressed viral antigens and thereby raising the important question (Asquith et al., 2000): 'Is HTLV-I infection really silent?' This issue has recently been resolved by Asquith et al. (2007), who have demonstrated experimentally that each day, a small proportion of infected target cells spontaneously re-activate and express viral antigens. Such studies have been crucial in establishing that the strategy of HTLV-I infection is not that of complete latency, but one that is more dynamic.

In light of our overall theme of understanding HTLV-I persistence, in this section, we consider the following conundrum: Why is HTLV-I not silent? Indeed, the expression of viral proteins accompanying infected T-cell activation exposes proviral cells to immune surveillance, resulting in the risk of destruction. If this is the case, then why would the evolution of HTLV-I favour a route for viral expression and activation rather than remaining completely latent? The fact is that viral activation can be both beneficial and detrimental to the proviral cell. On the one hand, displaying viral proteins is required for infectious cell-to-cell transmission and is believed to drive the rapid, selective expansion of infected cells (Asquith and Bangham, 2008; Igakura et al., 2003). On the other hand, it simultaneously allows such cells to be eliminated by a persistently activated HTLV-I-specific CTL response (Asquith et al., 2005; Bangham, 2003). The balance between the two opposing selection forces determines the outcome of infection. To resolve our conundrum, we switch our perspective to that of the virus to understand why and how viral activation can be advantageous.

Our mathematical model (1) explicitly incorporates the interactions among the latent and active states of HTLV-I proviral cells, and virus-specific CTLs. In particular, the transition from the latently infected target cell compartment to the actively infected target cell compartment is encapsulated in the parameter τ, the rate of spontaneous viral expression that accompanies proviral activation. We can therefore examine the impact of the parameter τ on the long-term behaviour of model (1). Our results are consistent with those of Li and Lim (2011), whose model explored in detail the role of Tax expression on chronic HTLV-I infection, but in the absence of a dynamically changing host immune response.

5.1.1. Tax/HBZ expression drives chronic infection and is an important determinant of proviral load

The basic reproduction number for viral infection R_0, defined in Eq. (2), can be thought of as a measure of viral success with respect to the ability to establish and propagate the infection. A simple computation shows that R_0 is an increasing function of τ; that is, the rate of spontaneous viral activation is seen to be a factor that drives the system towards chronic infection, making it difficult for infected individuals to clear the virus.

Next, we explore the way in which the expression of viral proteins affects the proviral load. In Fig. 3, we have plotted numerically a curve from our mathematical model (1) showing the impact of the rate τ of spontaneous infected target cell activation on the equilibrium proviral load v^*. Our model results show that for small values of τ, there is a sharp positive, rather than negative, correlation between τ and v^*. As the value of τ is increased, we observe that the magnitude of the proviral load v^* begins to level off before gradually decreasing and settling to a constant positive level for sufficiently large values of τ. Hence, viral expression is a factor that determines an infected individual's equilibrium proviral load. This second point provides further support for a non-latent virus strategy.

A traditional measure of viral success is the proviral load, and a higher proviral load is a better established infection. With this perspective, Fig. 3 can be thought of as reflecting a cost–benefit relationship for infected target cell activation that governs successful viral persistence: A rate of spontaneous viral expression that is too low is of little benefit to the virus as latency does not propagate the spread of infection; meanwhile, one that is too high could also be detrimental as it over-exposes proviral cells to host immunity and places a stronger demand on the virus to replicate

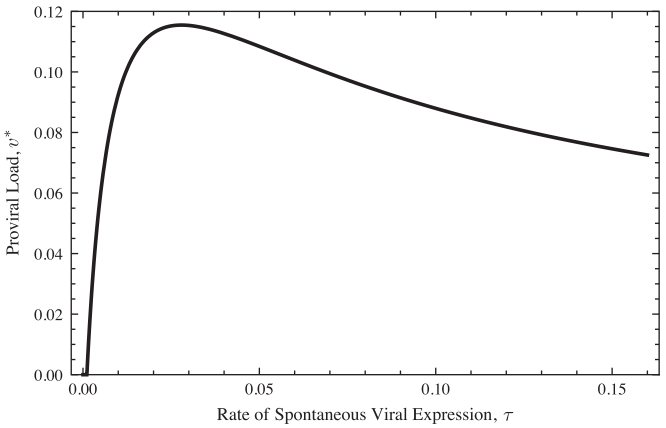

Fig. 3. The effect of spontaneous viral activation τ and subsequent expression of viral antigens on the equilibrium proviral load v^* as governed by our mathematical model (1). The above graph was obtained by solving the equilibrium equations for model (1) numerically using the parameter values from Table 1 to determine x^*, u^*, and y^*, then plotting the quantity $v^* = (u^*+y^*)/(x^*+u^*+y^*)$ as a function of the parameter τ.

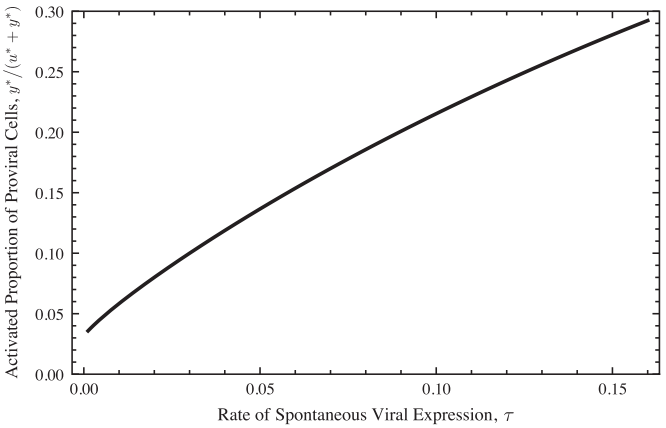

Fig. 4. A faster rate of proviral expression τ increases the proportion of infected target cells that are transcriptionally active $y^*/(u^*+y^*)$ at equilibrium. The above graph was obtained by determining the steady state solutions during chronic infection for model (1) numerically, then plotting the quantity $y^*/(u^*+y^*)$ as a function of the parameter τ. All parameter values have been selected from Table 1.

fast enough to outpace CTL-mediated lysis. Our results suggest that an intermediate rate of spontaneous infected T-cell activation, for example in the vicinity of the peak of the graph in Fig. 3, could be optimal for HTLV-I to successfully establish and maintain a high proviral load in the presence of host immunity. This observation supports the theoretical hypothesis by Asquith and Bangham (2008) that HTLV-I relies on a dynamic balance between viral latency and activation in order to persist indefinitely in the host: complete transcriptional latency is counter-productive to viral transmission and propagation of the infection, whereas full infected T-cell activation leaves too many proviral cells susceptible to immune-mediated lysis. Nevertheless, there may be another consequence of a higher rate of spontaneous viral protein expression despite its association with lowering the magnitude of the proviral load, which comes to light by examining the activated fraction of infected cells.

5.1.2. *Tax/HBZ expression increases activated fraction of infected cells*

Model (1) allows us to consider the effect of spontaneous viral expression or activation, represented by the parameter τ, on the second measure of viral burden or detriment, the equilibrium proportion of proviral cells that are actively infected, $y^*/(u^*+y^*)$. The result of numerical investigation of this dependence is shown in Fig. 4, where we observe that the net effect of a faster rate of spontaneous viral expression is a higher active proportion. In addition, unlike the proviral load v^*, which decreases when τ is sufficiently large, the active proportion of proviral cells is a monotonically increasing function of τ. The main implication of the result here is that the rate of spontaneous viral expression, τ, determines a characteristic ratio of latent versus activated infected cells at equilibrium, irrespective of the magnitude of the proviral load itself.

Our model predicts a relationship between the proviral load v^* and the active proportion of infected cells $y^*/(u^*+y^*)$ which is consistent with the recent experimental results by Melamed et al. (2013), who demonstrated a negative correlation between the abundance of a given infected T-cell clone and the proportion of the respective clone that spontaneously expresses the provirus in HAM/TSP patients. Taken together, the results shown in Figs. 3 and 4 imply such a negative correlation, when the rate of spontaneous viral expression τ exceeds a threshold value (of about 0.03 day^{-1} as in Fig. 3; see also Fig. B3 in Appendix B).

5.2. *Evaluating CTL quality: what determines the strength of the HTLV-I-specific CTL response, and why is infection life-long?*

In the previous section, we investigated the impact of spontaneous viral expression in our model to try and resolve the issue as to why HTLV-I is not silent. We have discovered that a low level of viral protein expression can offer tremendous benefits in terms of viral propagation and success. In other words, the net effect of viral activation is to drive chronic infection and aid the persistence of HTLV-I. These observations in turn suggest a complex interaction with the host immune response that we now explore in further detail.

5.2.1. *CTL frequency ≠ CTL efficiency*

It is well established that cellular immunity, driven by the selective expansion of anti-viral CTLs, is an important branch of the human immune system that aids in eliminating invading intracellular pathogens such as viruses (Parham, 2005). In the case of HTLV-I, virus-specific CTLs have been shown experimentally to be highly efficient at killing antigen-expressing proviral cells and are important determinants of an infected individual's proviral load (Asquith et al., 2005). Moreover, CTLs are thought to play a role in the development of HTLV-I-associated pathologies (Asquith and Bangham, 2000; Bangham et al., 1999; Jeffery et al., 1999), although there is conflicting speculation as to whether CTLs are protective or whether they contribute to disease progression (Biddison et al., 1997; Mosley and Bangham, 2009). It is therefore essential to investigate how CTLs affect the outcome of chronic HTLV-I infection.

The strength of the immune response against virally infected cells has traditionally been thought of as being directly related to the frequency or magnitude of virus-specific CTLs in the peripheral blood. In HTLV-I infection, large numbers of circulating anti-HTLV-I CTLs are often found in blood samples from HTLV-I seropositive individuals, whether or not malignant disease is present (Bangham, 2003; Biddison et al., 1997; Parker et al., 1992). Such an observation is somewhat unexpected as the vast majority of the proviral load is latent and therefore invisible to host immunity. Indeed, how is it possible for the CTL response to have any impact on the course of infection when most proviral cells are transcriptionally silent at any given time and are thus not even visible to immune surveillance? Asquith and Bangham (2008) hypothesise that since the expression of HTLV-I proteins is crucial for viral propagation, then by exerting selective pressure on the small proportion of

virus-expressing cells, CTLs block a key point in the virus life cycle and can therefore have a substantial effect on the infection dynamics.

This underlies an important issue that arises in experimental data on HTLV-I-infected individuals, which is identifying the aspects of cellular immunity that are responsible for controlling the proviral load during the chronic phase of infection. A natural question comes to mind: What determines CTL quality? Does the size of the CTL response influence its ability to reduce the proviral load?

We again turn to our mathematical model (1) for some insights, focussing on two specific factors commonly believed to impact the proviral load of an infected individual: CTL frequency and CTL-mediated lysis of antigen-expressing infected cells. In our model, the equilibrium proviral load is given by v^*. Moreover, the abundance of CTLs is precisely z^* and the rate at which CTLs eliminate activated proviral cells is represented by the parameter γ.

A few straightforward calculations in our model yield Theorem 5.1, which demonstrates that the proviral load is positively correlated with the level of CTLs at equilibrium and negatively correlated with the rate of CTL-mediated lysis. The proof may be found in Appendix A. What our result suggests is that the strength or efficacy of the CTL response with respect to controlling the proviral load is influenced by how fast the HTLV-I-specific CTL response can eliminate virus-infected target cells rather than how large the pool of such CTLs is. A significant implication of this result is that the traditional line of thinking that the strength of the anti-HTLV-I CTL response is equal to its size needs to be re-evaluated.

Theorem 5.1. *Assume that $R_0 > 1$. Then, the equilibrium proviral load v^* is an increasing function of z^*, but a decreasing function of γ.*

Intuitively, one may expect that the more CTLs there are, the stronger the immune response, and thus the lower the proviral load. However, the notion that large numbers of CTLs can be associated with large numbers of virus-infected cells is not new, and has been observed in clinical data (Kubota et al., 2000; Nagai et al., 2001; Wodarz et al., 2001). Moreover, experiments have demonstrated that a fast rate of clearance of virus-expressing infected cells is associated with a reduced proviral load (Asquith et al., 2005).

Fig. 5 shows a positive correlation between the frequency of HTLV-I-specific CTLs and the proviral load in an HTLV-I seropositive individual. In Fig. 5(a), the experimental data by Nagai et al. (2001) measured the percentage of CTLs targeting the immunodominant viral Tax protein in the context of HLA-A2 which represented the bulk of the anti-HTLV-I CTL response, and the viral burden was measured in terms of the number of proviral cells per 100 peripheral blood mononuclear cells (PBMCs), which is directly proportional to the number of $CD4^+$ helper T-cells that are infected. Meanwhile, Fig. 5(b) plots the relationship between the number of CTLs z^* at equilibrium and the proviral load v^* in terms of the infected fraction of target cells as determined by our mathematical model (1). Although quantitative comparisons have not been done, our theoretical results agree qualitatively with the experimental data from Nagai et al. (2001).

Fig. 6 displays a negative correlation between the rate at which actively infected target cells expressing viral antigens are cleared by $CD8^+$ CTLs, and the proviral load. Asquith et al. (2005) reported their experimental measurements of anti-viral efficacy as the number of Tax^+ cells cleared per day per CTL and its correlation with the proviral load in terms of PBMCs (Fig. 6(a)). As Tax is the immunodominant viral antigen targeted by CTLs, such a measure is directly related to the parameter γ in our model. In addition, the viral burden measured in terms of infected PBMCs corresponds

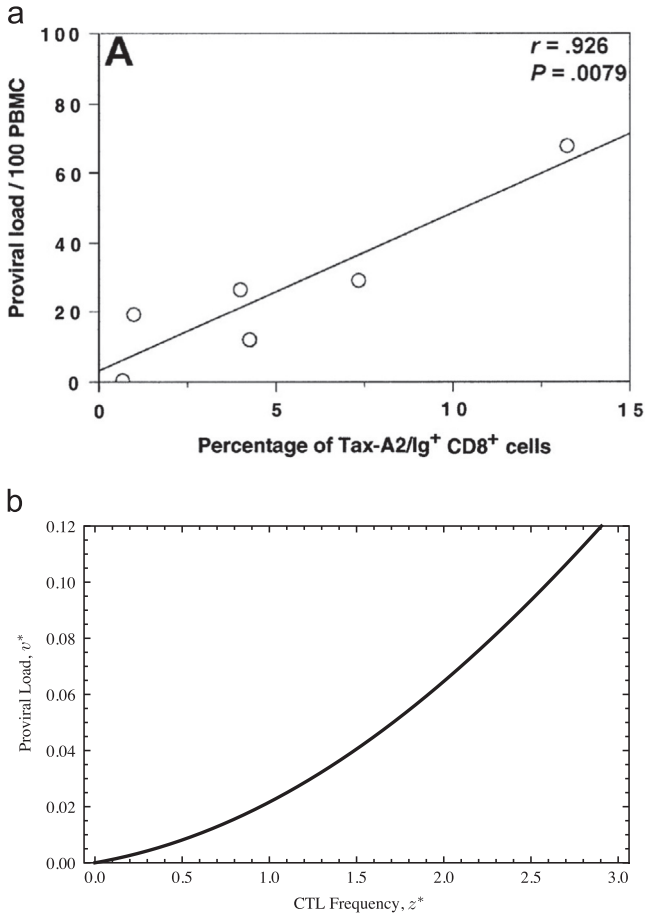

Fig. 5. Positive correlation between CTL frequency (horizontal axis) and proviral load (vertical axis). (a) The experimental results from Nagai et al. (2001) show data points and have been fitted theoretically with a linear curve. (Figure reproduced with permission from the publisher.) (b) The corresponding curve from our model (1), which plots the relationship between the proviral load v^* and CTL abundance z^* at equilibrium, displays a different form, but agrees qualitatively with the experimental data. Parameter values have been selected as in Table 1.

directly to the measure of the proviral load with respect to the $CD4^+$ helper T-cell population, which is represented in our model by the quantity v^*. We observe that the data from Asquith et al. (2005) are in qualitative agreement with Fig. 6(b), which shows how the equilibrium proviral load v^* changes with respect to γ according to our mathematical model (1).

Our model therefore supports the relatively recent idea that a large CTL response is not necessarily a strong one, and that CTL frequency is not a reliable measure of immune efficiency (Bangham, 2009; Bangham et al., 1999). In addition, our findings agree with previous mathematical modelling work by Nowak and Bangham (1996) and Wodarz et al. (2001) demonstrating how the CTL response to persistent viral infections such as HIV and HTLV-I can be inefficient at controlling the proviral load yet CTLs may exist in abundance.

5.2.2. *Efficient CTLs cannot eliminate the active proportion of proviral cells*

We have shown that effective immune control of the HTLV-I proviral load is reflected in the rate at which CTLs eliminate actively infected cells rather than the size of the CTL pool. This finding motivates the question: Why is there no cure for HTLV-I infection? Indeed, our results indicate that a fast rate of CTL-mediated lysis is effective at reducing the proviral load. Yet, the

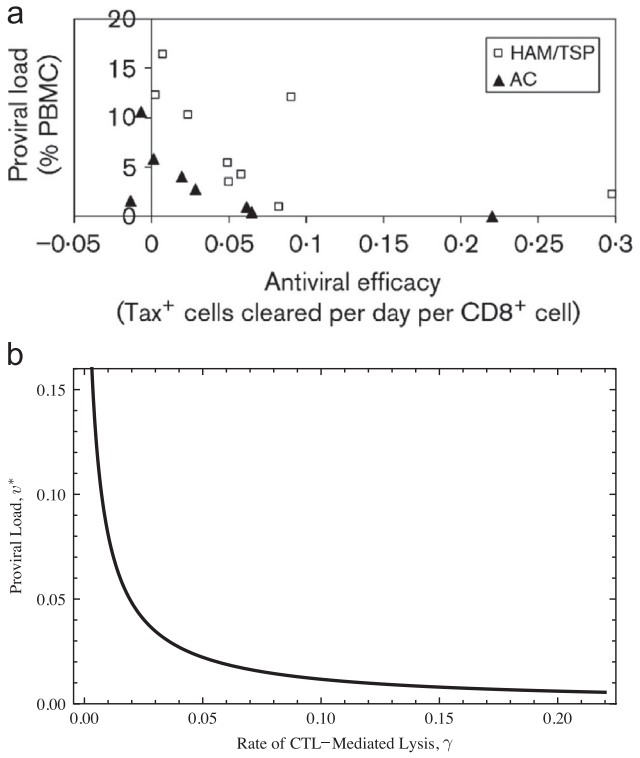

Fig. 6. Negative correlation between rate of CTL-mediated lysis (horizontal axis) and the proviral load (vertical axis). (a) The experimental measurements from Asquith et al. (2005) show data points for both ACs and HAM/TSP patients. (Figure reproduced with permission from the publisher.) (b) Our model results arising from the system of Eq. (1) are in qualitative agreement. Parameter values are taken from Table 1.

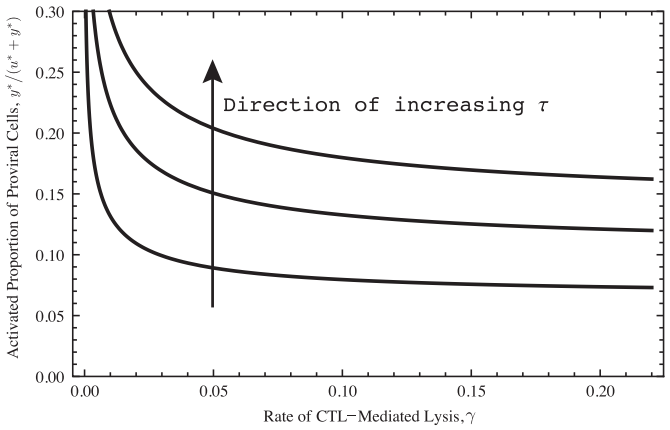

Fig. 7. Evaluating the effects of γ and τ on $y^*/(u^*+y^*)$ in model (1). CTL quality or effectiveness may be characterised by high values of γ. For fixed values of τ, when γ is sufficiently large, a further increase in γ has little effect on the Tax^+/HBZ^+ proportion of proviral cells, $y^*/(u^*+y^*)$. Therefore, even though efficient CTLs reduce the magnitude of the proviral load, they do not necessarily decrease the active (i.e. 'aggressive') proportion of proviral cells.

application of vaccines that boost the efficiency of CTL responses elicited by infected hosts has been unsuccessful at achieving complete elimination of the virus, and infection remains chronic (Bangham, 2000).

Using our mathematical model (1), we offer a possible explanation for this failure by examining the impact of CTL efficiency, encapsulated by the parameter γ, on the proportion of proviral cells that is activated, $y^*/(u^*+y^*)$. We observe from numerical investigations that for sufficiently large values of γ, further changes in γ have little effect on the active proportion of proviral cells (note that we can equally conclude from the results shown in Fig. 6(b) that, when this same value of γ is exceeded, there is little further reduction in the proviral load v^*). Indeed, combining this result with our earlier finding that the rate of spontaneous viral expression τ displays a positive correlation with the active proportion of proviral cells yields Fig. 7, which illustrates that the quantity $y^*/(u^*+y^*)$ steadily increases with larger values of τ for fixed values of γ, whereas for fixed τ, an increase in γ has only a minimal impact on $y^*/(u^*+y^*)$ when γ is sufficiently large.

The main implications of the above result are the following: (1) an efficient CTL response fails to eradicate the infection because it cannot eliminate the activated (i.e. 'aggressive') part of the infected target cell population, and (2) a faster rate of proviral activation which exposes more infected cells to immune surveillance makes it more difficult for CTLs to achieve clearance of activated proviral cells. These observations motivate a hypothesis relating to pathogenesis which is discussed in the following section.

5.3. *Insights to HTLV-I-associated disease: what characterises HTLV-I-linked pathology?*

A puzzling issue in HTLV-I infection is why only a small fraction of chronically infected individuals develop the inflammatory disease HAM/TSP whereas the vast majority remains as life-long asymptomatic carriers (ACs) of the virus. Although much experimental work has shed light on the way in which several key factors of the infection may be associated with clinical status, either AC or HAM/TSP patient, a clear determinant to distinguish between the two states is not yet known.

In the previous sections, our investigations of key factors including spontaneous activation of proviral cells, CTL frequency, and CTL efficiency have illuminated important properties of HTLV-I infection that help our understanding of viral persistence in the presence of chronically activated immune responses. In this section, we take our results one step further by interpreting the roles of these key parameters in the context of HTLV-I-associated disease. In particular, we propose a plausible hypothesis for the identification of disease status and suggest a possible mechanism for pathogenesis.

5.3.1. *A hypothesis for determining clinical status*

The equilibrium proviral load is a major correlate of clinical status: a high proviral load is associated with HAM/TSP development, whilst a low proviral load is associated with asymptomatic carriage. However, it is known that the size of the proviral load does not, on its own, separate ACs from HAM/TSP patients. Indeed, there is broad overlap among the proviral loads of ACs and HAM/TSP patients, and a high proviral load is not a reliable determinant of disease status (Asquith and Bangham, 2007; Asquith et al., 2005).

We propose instead that the extent of activation of proviral cells, $y^*/(u^*+y^*)$, and not necessarily the absolute magnitude of the proviral load, v^*, may be associated with the inflammatory disease, HAM/TSP. For example, there may be a threshold level for the activated proportion of infected target cells above which asymptomatic carriers develop disease, regardless of the size of the proviral load. This hypothesis for distinguishing between ACs and HAM/TSP patients is shown graphically in Fig. 8(a), where the proposed theoretical threshold for pathogenesis is represented by the thin, horizontal dotted line. Our hypothesis is consistent with previous experimental data showing that infected cells from HAM/TSP patients expressed the Tax protein at higher levels than those from ACs (c.f. Fig. 2 from Asquith et al., 2005).

In chronic HTLV-I infection, it is well-documented that the magnitude of the proviral load is not a direct reflection of the

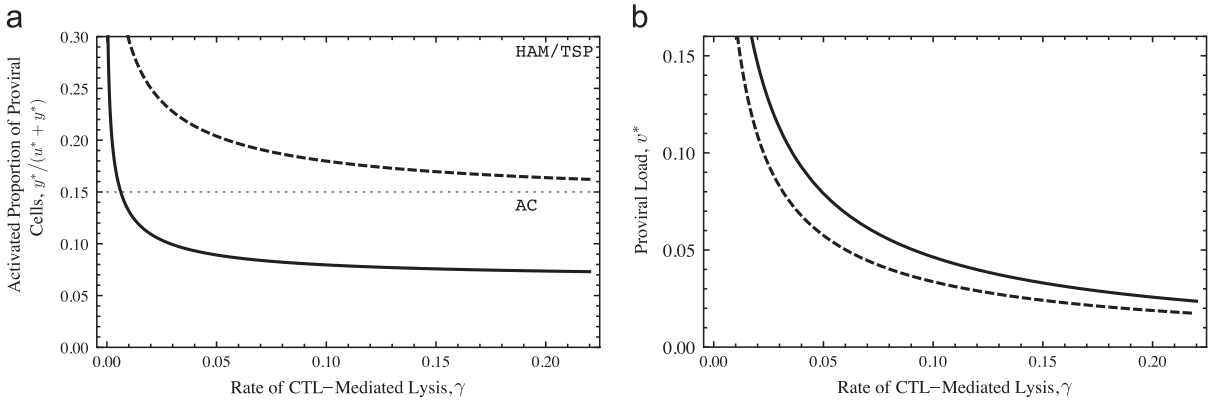

Fig. 8. A hypothesis for classifying clinical status arising from our mathematical model (1) is that a high activated proportion of infected cells and not necessarily the size of the proviral load may be an important determinant of disease. In the above figures, the solid line and the dashed line correspond to two different individuals. The individual represented by the solid line is seen to have a lower activated proportion of infected cells, but a higher proviral load, than that of the individual represented by the dashed line. Furthermore, for sufficiently high rates of CTL-mediated lysis γ, the individual corresponding to the solid line has an active proportion of infected cells that lies below the theoretical threshold for disease manifestation and would therefore be classified as an asymptomatic carrier under our hypothesis, despite having a higher absolute magnitude of the proviral load than the individual corresponding to the dashed line. (a) The thin horizontal dotted line indicates a theoretical threshold for disease manifestation. (b) A high proviral load is neither necessary nor sufficient to identify the presence of disease.

extent of activation of proviral cells. Although generally a high proviral load is associated with disease progression, it is not uncommon for asymptomatic carriers to harbour proviral loads that are higher than those of symptomatic carriers (Asquith et al., 2005). The separation of clinical status based on the active proportion of infected target cells rather than the magnitude of the proviral load could potentially explain how infected individuals with a low proviral load could have HAM/TSP due to a high proportion of activated infected cells, or conversely, how those with a high proviral load could be asymptomatic due to a low proportion of activated infected cells. For a wide range of parameter values, our model exhibits behaviour that is consistent with experimental observations (c.f. Fig. 2(b) from Asquith and Bangham, 2008); that is, at a given rate of CTL lysis, the proviral load in ACs is lower than that in HAM/TSP patients (results not shown). However, due to the shape of the curve describing how the activated proportion of infected cells changes with the proviral load and because the proposed theoretical threshold for disease manifestation is not precisely known, our model can also exhibit the converse phenomenon in which the proviral load in an AC is greater than that of a HAM/TSP patient (for more details, we refer the reader to Figs. 3 and 4, as well as Fig. B3 in Appendix B). Indeed, such a scenario is possible in our model as highlighted in Fig. 8, where we have plotted the efficiency of the CTL response γ against the two different measures of viral detriment. Parameter values are selected that lie in the same range as those in Table 1. In Fig. 8(a), with respect to the activated proportion of proviral cells, the solid line lies below the threshold for pathogenesis for all sufficiently large values of γ, and thus corresponds to asymptomatic clinical status, while the dashed line lies above the proposed threshold for all γ and would therefore represent a patient with HAM/TSP. Yet with respect to the proviral load v^* as in Fig. 8(b), it is seen that for all values of γ, the magnitude of v^* for the AC (given by the solid line) is, in fact, higher than that for the HAM/TSP patient (given by the dashed line). Our model therefore allows for a consistent framework that could potentially account for the existence of this phenomenon if it were to occur. Further studies are needed to deduce better estimates for the position of the theoretical threshold for disease manifestation and determine if such a scenario is possible, i.e. can there exist two HTLV-I seropositive individuals with the same immune efficiency, one AC and one HAM/TSP patient, in which the proviral load of the AC is higher than that of the HAM/TSP patient?

5.3.2. *Failure of HAM/TSP treatment*

We have observed previously how increasing the rate of CTL-mediated lysis γ, which is a measure of CTL efficiency, is effective in lowering the magnitude of the proviral load, but is ineffective in reducing the activated proportion of infected target cells. In terms of the efficiency of the CTL response, there is an additional consequence of our hypothesis for identifying clinical status. Taking another look at Fig. 8(a), we notice that it is possible for chronically infected individuals to have less efficient CTLs (i.e. a low value of γ) and still be asymptomatic because of having an active proportion of infected cells that lies below the designated threshold. Alternatively, it may also happen that chronically infected individuals with very efficient CTLs (i.e. a high value of γ) could be diagnosed with HAM/TSP due to an active proportion of infected cells that lies above the proposed threshold.

The above observation has an implication for HAM/TSP treatments and could offer a possible explanation as to why a cure for the disease has been difficult to discover. Consider an infected individual with HAM/TSP who has a given immune efficiency γ, as indicated by the open circle in Fig. 9. The dashed line shows how the activated proportion of proviral cells of this individual (i.e. with all other parameters fixed) varies with different rates of CTL-mediated lysis. Suppose that treatment is administered that enhances the efficiency of the HTLV-I-specific CTL response, which although lowering the absolute magnitude of the proviral load v^* does not significantly impact the proportion of proviral cells that are actively infected. The active proportion continues to lie above the threshold for pathogenesis and the individual remains with the inflammatory disease.

5.3.3. *Immune compromise is a possible though unlikely cause of disease*

An intriguing aspect of chronic HTLV-I infection is that only a small fraction of infected individuals develop the inflammatory disease, HAM/TSP, after a long asymptomatic clinical phase. It remains unresolved as to how or why disease may manifest over time during the chronic stage of infection. In the context of our hypothesis, if there does exist a threshold level for the activated proportion of infected target cells that distinguishes clinical status, how could it be possible for the active proportion to increase and eventually cross the proposed threshold?

One possible route, which occurs in HIV infection, is that the virus severely compromises the human immune system, and

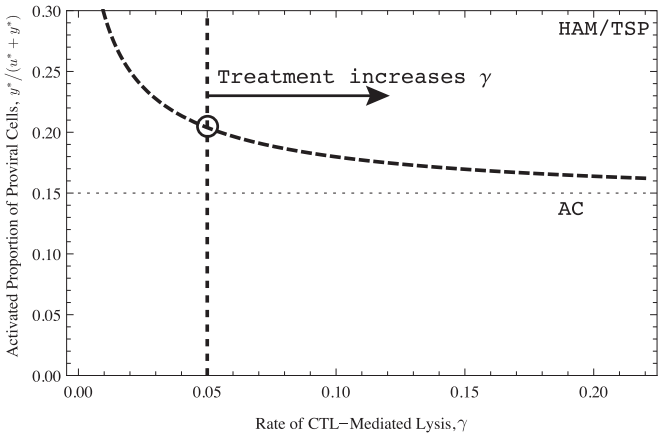

Fig. 9. Failure of HAM/TSP treatment. Results from our mathematical model (1) suggest a plausible reason as to why treatment for HTLV-I pathology is unsuccessful. Although the administration of vaccines that improves the efficiency of anti-HTLV-I CTLs reduces the magnitude of the proviral load, it may be ineffective at lowering the activated proportion of proviral cells below the theoretical threshold for pathogenesis.

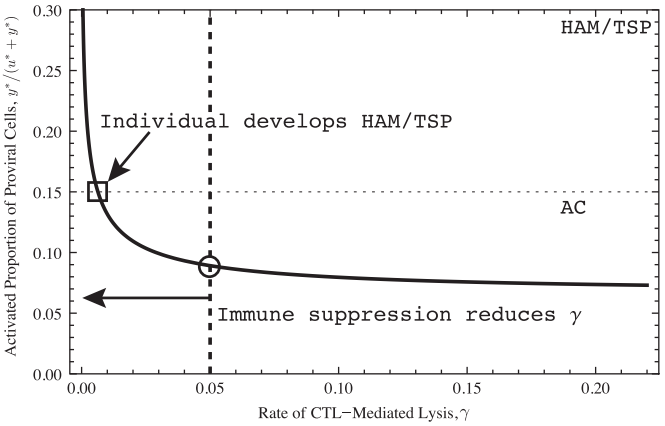

Fig. 10. A prediction of model (1) is that immune compromise leading to development of disease is possible. However, chronic infection by HTLV-I is not associated with immune suppression, suggesting that such an explanation for disease progression is unlikely.

a weakened state allows for the progression of disease. For instance, over time HTLV-I may disrupt the functionality of the immune system and render virus-specific CTLs ineffective at controlling viral replication, allowing the population of proviral cells to expand tremendously. The scenario is illustrated in Fig. 10, where we first consider an asymptomatic carrier with a given rate of CTL-mediated lysis γ, represented by the open circle. The solid black line shows how the active proportion of proviral cells varies with respect to immune efficiency γ and all other parameters fixed. It is reasonable to believe that as time progresses, the efficiency of the CTL response is compromised so that the value of γ becomes very small. In this case, the active proportion of the viral burden would increase and could end up above the threshold for pathogenesis, which is shown in Fig. 10 as an open square. The infected individual then develops HAM/TSP. However, it has been experimentally shown that chronic infection by HTLV-I is not associated with overt immuno-suppression (Asquith and Bangham, 2007); more or less normal T-cell functionality remains. If anything, the efficiency of a functional CTL response is thought to increase over time, rather than decrease, due to continued exposure and increased specificity towards target antigens (Parham, 2005). This explanation is therefore unlikely to describe the progression of HAM/TSP.

5.3.4. A plausible mechanism for pathogenesis

Although silencing the expression of viral proteins allows HTLV-I to evade immune selection, there is little benefit for proviral cells to be fully transcriptionally latent. Indeed, continued propagation of the infection requires that at least a small fraction of latently infected cells becomes spontaneously re-activated each day. As we have seen previously in Fig. 4, the rate of spontaneous infected T-cell activation, τ, displays a strict positive correlation with the active proportion of proviral cells, $y^*/(u^*+y^*)$. In terms of the development of the inflammatory disease, HAM/TSP, we offer a hypothesis that as time progresses, the active proportion of proviral cells may increase, and could eventually cross the threshold for pathogenesis, thus causing disease. One way that this could happen is that the rate τ of spontaneous expression of viral proteins, which in our model is treated as a constant, may in fact increase over time.

A hypothetical situation is illustrated in Fig. 11. As before, we consider an asymptomatic carrier with a specified CTL efficiency γ. The position of this individual is given by the open circle on the graph, and the solid black curve on which the open circle lies is the way that the active proportion of proviral cells changes with respect to the rate of CTL-mediated lysis, γ, with all other parameters fixed. Suppose that over time, the rate of spontaneous infected target cell activation τ increases. The net effect, as expected, would be a general increase in the active proportion of infected cells. It is then possible that the proportion of actively infected cells reaches the threshold for pathogenesis, represented by the open square in Fig. 11, and manifestation of the inflammatory disease, HAM/TSP, occurs.

However, it is known that the vast majority of chronically infected individuals do not develop HAM/TSP, and instead remain asymptomatic throughout their lifetime. Supposing our hypothesis on the threshold for pathogenesis is true, this suggests that either the proposed threshold for the activated proportion of proviral cells is much higher than that of most HTLV-I-infected individuals or that perhaps τ does not change significantly over the course of chronic infection. Nevertheless, it is not clear why the rate of spontaneous viral expression τ would increase over time. Indeed, this rate is thought to be characteristic to each individual and is determined by two primary factors that remain relatively constant over time: the HTLV-I genomic sequence, which is genetically stable, and the dominance of infected T-cell clones, each defined by a specific site of integration into the host DNA (Bangham et al., 2009; Gillet et al., 2011; Meekings et al., 2008). Further studies are needed to resolve these issues and test the validity of our hypothesis.

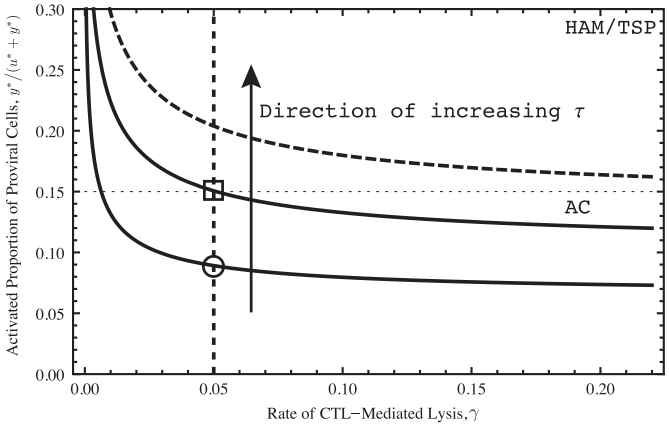

Fig. 11. Our mathematical model (1) suggests a plausible mechanism for the development of disease. An increase in viral protein expression over the course of chronic HTLV-I infection may eventually push the active proportion of proviral cells over the proposed threshold for pathogenesis.

6. Biological conclusions

In this paper, we have developed a theoretical framework that incorporates sufficient biological complexity to accurately describe the fundamental within-host dynamics of HTLV-I infection and, at the same time, is able to account for some of the idiosyncrasies frequently observed in HTLV-I experimental and clinical data. Specifically, we have investigated our mathematical model (1) in the context of several important questions regarding the persistence and pathogenesis of HTLV-I in order to gain some biologically meaningful insights into the nature of chronic HTLV-I infection. One key feature of our model that differs from previous models is the consideration of a dynamically changing within-host environment involving the complex interplay between infected target cells that may either be latent or activated, and persistent virus-specific host immune responses. Our study has shed light on the way in which HTLV-I interacts with host immunity to persist. The results of our model are consistent with experimental observations and, in addition, raise further questions that may be experimentally testable.

In particular, we set out to illuminate the following three key questions in HTLV-I immunology:

Q1. *Why is HTLV-I not silent?*

- *Viral expression is necessary for the establishment, propagation, and persistence of HTLV-I infection.*

  Recently, Asquith et al. (2007) have given a definitive resolution to the issue of HTLV-I latency by demonstrating experimentally that HTLV-I is not a fully silent infection and that on-going viral transcription is present. We asked the question: Why is HTLV-I not silent since proviral activation exposes infected target cells to immune-mediated pressure?

  We investigated this question in the context of our mathematical model, and discovered that for a completely latent virus, the benefits gained by activation aided in the establishment of infection. Moreover, the rate of spontaneous expression of viral antigens was shown to be an important determinant of the proviral load.

Q2. *What determines the strength of the HTLV-I-specific CTL response, and why is infection life-long?*

- *Efficient control of the HTLV-I proviral load depends on a high rate of CTL-mediated lysis and not on the frequency of anti-HTLV-I CTLs.*

  Our model has demonstrated that despite frequent viral latency, the HTLV-I-specific CTL response is a factor that determines the level of the proviral load at equilibrium. The ability of the CTL response to effectively control the proviral load may not be dependent upon the numbers of CTLs, but on how fast CTLs are able to lyse the relatively small proportion of virus-infected target cells that are activated. The results of our model agree qualitatively with experimental data from Nagai et al. (2001) and Asquith et al. (2005).

- *Infection may be life-long because efficient immune responses fail to eliminate the small proportion of proviral cells that are activated.*

  An efficient HTLV-I-specific CTL response kills virus-expressing actively infected cells at a rapid rate and lowers the proviral load. However, due to the benefits to the virus gained by exhibiting at least a low level of proviral expression, a plausible reason why efficient CTLs cannot eradicate the infection is because they are unable to completely eliminate the activated proportion of proviral cells that are aggressively propagating the infection. Furthermore, from our model, we have shown the somewhat non-intuitive result that a faster rate of spontaneous proviral activation and subsequent expression of HTLV-I antigens, which exposes more infected target cells to host immunity, make it more challenging for CTLs to achieve complete viral clearance of the actively infected target cell pool.

Q3. *What characterises HTLV-I-linked pathology?*

- *The extent of proviral activation rather than the size of the proviral load may distinguish clinical status and suggests a potential route for disease manifestation.*

  Finding a quantifiable measure for the amount of detriment caused by HTLV-I is important in assessing the severity of infection and disease: For an asymptomatic carrier, what is the risk of developing disease? For a HAM/TSP patient, how far has the disease progressed?

  A traditional measure of viral burden is the proviral load, which is a direct representation of the magnitude of the infection. However, the proviral load among both ACs and HAM/TSP patients can display large overlap and its magnitude alone cannot determine clinical status (Asquith et al., 2000; Mosley et al., 2005). We propose that the activated proportion of proviral cells could be an alternative measure of viral burden that distinguishes ACs from HAM/TSP patients, independent of the size of the proviral load. Namely, we hypothesise that a high level of infected target cell activation could be associated with HAM/TSP, whereas a low level of proviral activation may correspond to asymptomatic carriage—there exists a threshold level of activation separating the two states. Our results offer insights to two unknown issues in HTLV-I pathogenesis. (i) Why do HAM/TSP treatments fail to eradicate disease? and (ii) what causes the progression of HTLV-I infection from the asymptomatic stage to HAM/TSP?

  For the former, we have demonstrated using our mathematical model that treatments boosting the efficiency of the HTLV-I-specific CTL response may be inadequate at reducing the activated proportion of proviral cells below the proposed threshold level for disease, despite being effective at lowering the proviral load. For the latter, we suggest a plausible mechanism for disease manifestation: The rate of spontaneous viral activation increases over time, for example through activation induced by pro-stimulatory signalling pathways (Höllsberg et al., 1999), gradually raising the proportion of infected target cells that are activated and eventually crossing the proposed threshold for disease.

Acknowledgements

A.G. Lim acknowledges the financial support of scholarships from the Natural Sciences and Engineering Research Council of Canada (NSERC), the Alberta Heritage Scholarship Fund (AHSF), and the Canadian Centennial Scholarship Fund (CCSF). We thank Sunetra Gupta for helpful discussions throughout the preparation of the manuscript. We are also very grateful for the comments and critique from two anonymous referees which have helped to improve the clarity of the manuscript.

Appendix A. Proofs

A.1. Biologically realistic region

Proof of Theorem 3.1. It can be seen from the model equations that for any set of non-negative initial conditions, $x(t), u(t), y(t), z(t) \geq 0$ for

all $t \geq 0$. It is clear that

$$\frac{dx}{dt} \leq \lambda - \mu_1 x,$$

and this implies that

$$\limsup_{t\to\infty} x(t) \leq \frac{\lambda}{\mu_1}.$$

Adding the first three equations yields

$$\frac{d}{dt}(x+u+y) \leq \lambda - (\mu - r)(x+u+y),$$

where $\mu = \min\{\mu_1, \mu_2, \mu_3\}$, which implies that $\limsup_{t\to\infty}(x(t)+u(t)+y(t)) \leq \lambda/(\mu - r)$. The assumption that $r < \mu$ ensures that the quantity on the right-hand side of the inequality is always positive. For the last inequality, let $(x(t), u(t), y(t), z(t))$ be a solution of model (1) with $x(0)+u(0)+y(0) \leq \lambda/(\mu - r)$. Then,

$$\frac{dz}{dt} = \nu y - \mu_4 z \leq \nu \frac{\lambda}{\mu - r} - \mu_4 z \quad \Longrightarrow \limsup_{t\to\infty} z(t) \leq \frac{\lambda\nu}{\mu_4(\mu - r)}.$$

Therefore, we consider the closed, bounded region

$$\Gamma := \left\{ (x,u,y,z) \in \mathbb{R}^4_+ : x \leq \frac{\lambda}{\mu_1}, x+u+y \leq \frac{\lambda}{\mu - r}, z \leq \frac{\lambda\nu}{\mu_4(\mu - r)} \right\}.$$

It is a straight-forward exercise to verify that Γ is positively invariant in $\mathbb{R}^4$ and hence model (1) is well-posed.

A.2. Proof of Theorem 3.2. Part 1: existence of equilibria

The first proposition shows that the basic reproduction number for viral infection, given by

$$R_0 = \frac{\tau}{\mu_3(\tau+\mu_2)}(\beta x_H + r) \quad \text{where } x_H = \frac{\lambda}{\mu_1},$$

as in Eq. (2), determines the existence of equilibria in $\overline{\Gamma}$.

Proposition A1 (*Existence of equilibria*).

(1) *The infection-free equilibrium* $P_0 = (x_H, 0, 0, 0)$, *where* $x_H = \lambda/\mu_1$, *always exists in* $\overline{\Gamma}$. *Moreover, if* $0 < R_0 < 1$, *then* P_0 *is the only equilibrium in* $\overline{\Gamma}$.
(2) *If* $R_0 > 1$, *then there exist exactly two equilibria,* P_0 *on* $\partial\Gamma$ *and a unique chronic infection equilibrium* $P^* = (x^*, u^*, y^*, z^*)$ *in* Γ.

Proof. Equilibria occur when

$$0 = \lambda - \beta x y - \mu_1 x, \tag{A.1a}$$

$$0 = \beta x y + r y - (\tau + \mu_2) u, \tag{A.1b}$$

$$0 = \tau u - \gamma y z - \mu_3 y, \tag{A.1c}$$

$$0 = \nu y - \mu_4 z. \tag{A.1d}$$

Observe that since x, u, y, z are restricted to be non-negative in the biologically feasible region Γ, then from Eqs. (A.1c) and (A.1d), $u = 0 \Longleftrightarrow y = 0 \Longleftrightarrow z = 0$ at equilibrium. There are only two possible non-negative equilibria in our model (1): P_0 representing the infection-free state, and P^* representing chronic infection.

We first determine the existence of the *infection-free* equilibrium $P_0 = (x_H, 0, 0, 0)$, where $x_H = \lambda/\mu_1$ is the level of target cells in the absence of an infection and coincides precisely with the normal $CD4^+$ helper T-cell count in a healthy individual.

Next, we search for steady state solutions of the form $P^* = (x^*, u^*, y^*, z^*)$, where $x^*, u^*, y^*, z^* > 0$. We will refer to such a steady state, if it exists, as a *chronic infection* equilibrium. Eqs. (A.1a)–(A.1d) allow us to express x^*, u^*, and y^* in terms of z^*. Namely,

$$x^* = \frac{\lambda\nu}{\beta\mu_4 z^* + \nu\mu_1}, \quad u^* = \frac{\mu_4}{\tau\nu}(\gamma z^* + \mu_3) z^*, \quad y^* = \frac{\mu_4}{\nu} z^*, \tag{A.2}$$

where z^* is a root of the following function:

$$F(z) = \frac{\tau}{\mu_3(\tau+\mu_2)}\left(\frac{\beta\lambda\nu}{\beta\mu_4 z + \nu\mu_1} + r\right) - \frac{\gamma}{\mu_3} z - 1. \tag{A.3}$$

Clearly, $F(z)$ is a monotonically decreasing function of z and $\lim_{z\to\infty} F(z) < 0$. Moreover, since

$$F(0) = [R_0 - 1],$$

the existence of a unique positive root z^* of $F(z) = 0$ is equivalent to the condition that $R_0 > 1$, thus completing the proof. □

A.3. Proof of Theorem 3.2. Part 2: stability of P_0

The *Jacobian matrix* for model (1) is

$$J(x,u,y,z) = \begin{bmatrix} -\beta y - \mu_1 & 0 & -\beta x & 0 \\ \beta y & -\tau - \mu_2 & \beta x + r & 0 \\ 0 & \tau & -\gamma z - \mu_3 & -\gamma y \\ 0 & 0 & \nu & -\mu_4 \end{bmatrix}. \tag{A.4}$$

The local stability of P_0 is given by the following.

Proposition A2 (*Local stability of* P_0).

(i) *When* $R_0 < 1$, *the infection-free equilibrium* $P_0 = (x_H, 0, 0, 0)$, *where* $x_H = \lambda/\mu_1$, *is always locally asymptotically stable in the feasible region* Γ.
(ii) *When* $R_0 > 1$, P_0 *is unstable. Specifically,* P_0 *is a saddle with* $\dim W^s_{loc}(P_0) = 3$ *and* $\dim W^u_{loc}(P_0) = 1$, *where* $W^s_{loc}(P_0)$, $W^u_{loc}(P_0)$ *denote the local stable and unstable manifolds of* P_0, *respectively*.

Proof. Establishing the local stability of the infection-free equilibrium P_0 is equivalent to determining the signs of the real parts of the eigenvalues of $J(P_0)$, the Jacobian matrix at P_0. The characteristic polynomial is

$$\chi_0(\zeta) = (\zeta + \mu_1)(\zeta + \mu_4)[\zeta^2 + (\tau + \mu_2 + \mu_3)\zeta - \mu_3(\tau + \mu_2)[R_0 - 1]],$$

where R_0 is the basic reproduction number for viral infection defined in Eq. (2). The roots of $\chi_0(\zeta)$ are precisely the eigenvalues of the Jacobian matrix $J(P_0)$. They are given by $\zeta_i \in \mathbb{C}$ such that $\chi_0(\zeta_i) = 0$:

$$\zeta_1 = -\mu_1, \quad \zeta_2 = -\mu_4,$$

and

$$\zeta_{3,4} = -\tfrac{1}{2}(\tau + \mu_2 + \mu_3) \pm \tfrac{1}{2}\sqrt{(\tau + \mu_2 + \mu_3)^2 + 4\mu_3(\tau + \mu_2)[R_0 - 1]}.$$

Clearly, both $\zeta_1, \zeta_2 < 0$. Moreover, if $R_0 < 1$, then $\mathrm{Re}(\zeta_3), \mathrm{Re}(\zeta_4) < 0$. Hence P_0 is either a stable node or a stable spiral. However, if $R_0 > 1$, it is readily seen that $\mathrm{Re}(\zeta_3) > 0$, so that P_0 is unstable. Specifically, P_0 is a saddle whose local stable manifold $W^s_{loc}(P_0)$ has dimension 3 and local unstable manifold $W^u_{loc}(P_0)$ has dimension 1. If $R_0 = 1$, $\zeta_3 = 0$ is a zero eigenvalue of $J(P_0)$ and no immediate conclusions about the local stability of P_0 may be inferred. The preceding argument establishes the basic reproduction number for viral infection R_0 as a threshold parameter that characterises the local stability of the infection-free equilibrium P_0. □

In fact, a stronger statement can be made about the stability of P_0 when $R_0 < 1$, namely that it is globally asymptotically stable in the feasible region Γ.

Proposition A3 (*Global stability of P_0*). *When $R_0<1$, the infection-free equilibrium P_0 is globally asymptotically stable in the feasible region Γ.*

Proof. Assume that $R_0<1$. Then by Proposition A1, the infection-free steady state P_0 is the only equilibrium point in $\overline{\Gamma}$. Note that $x\le x_H$ for all $x\in\Gamma$.

Consider

$$L=L(x,u,y,z)=\left(x-x_H-x_H\log\frac{x}{x_H}\right)+u+\frac{\tau+\mu_2}{\tau}y+\frac{\gamma(\tau+\mu_2)}{2\tau\nu}z^2.$$

The function $L:\mathbb{R}^4_+\to\mathbb{R}$ is positive definite, as

(i) $L(x_H,0,0,0)=0$, i.e. $L(P_0)=0$; and
(ii) $L(x,u,y,z)>0$, for all $(x,u,y,z)\in\mathbb{R}^4_+,(x,u,y,z)\neq(x_H,0,0,0)$.

The Lyapunov derivative of L is

$$\begin{aligned}\frac{dL}{dt}&=\left(1-\frac{x_H}{x}\right)\frac{dx}{dt}+\frac{du}{dt}+\frac{\tau+\mu_2}{\tau}\frac{dy}{dt}+\frac{\gamma(\tau+\mu_2)}{\tau\nu}z\frac{dz}{dt}\\&=\left(1-\frac{x_H}{x}\right)(\lambda-\mu_1x)-\beta xy\left(1-\frac{x_H}{x}\right)\\&\quad+(\beta xy+ry-(\tau+\mu_2)u)+\frac{\tau+\mu_2}{\tau}(\tau u-\gamma yz-\mu_3y)\\&\quad+\frac{\gamma(\tau+\mu_2)}{\tau\nu}z(\nu y-\mu_4z).\end{aligned}$$

Replacing $\lambda=\mu_1x_H$ and expanding terms yield

$$\begin{aligned}\frac{dL}{dt}&=-\frac{\mu_1}{x}(x-x_H)^2+\frac{\mu_3}{\tau}(\tau+\mu_2)[R_0-1]y-\frac{\gamma\mu_4}{\tau\nu}(\tau+\mu_2)z^2\\&\le 0,\quad\forall(x,u,y,z)\in\Gamma\text{ since }R_0<1.\end{aligned}$$

Hence, L is an appropriate Lyapunov function and moreover, $dL/dt(x_H,0,0,0)=L(x_H,0,0,0)=0$. Since the feasible region Γ is compact and invariant with respect to the vector field of model (1), it then follows from LaSalle's (1976) invariance principle that every trajectory starting in Γ approaches a set M, where M is the largest invariant subset of

$$I=\left\{(x,u,y,z)\in\mathbb{R}^4_+:\frac{dL}{dt}(x,u,y,z)=0\right\},$$

which, in the present case, is precisely

$$\{x\equiv x_H\}\cap\{y\equiv 0\}\cap\{z\equiv 0\}.$$

To establish the global stability of P_0 when $R_0<1$, it remains to show that the set M consists solely of the equilibrium point P_0. Observe that in the set I, the variable u can take on any arbitrary value along the non-negative real line. Let $\omega(t')=(x(t'),u(t'),y(t'),z(t'))$ be any trajectory of model (1) starting in I, so that $x(0)=x_H$, $y(0)=0$, and $z(0)=0$. Then, the behaviour of $\omega(t')$ at $t'=0$ is governed by

$$\frac{dx}{dt}=0,\quad\frac{du}{dt}=-(\tau+\mu_2)u,\quad\frac{dy}{dt}=\tau u,\quad\frac{dz}{dt}=0.$$

Hence, $x(t')\equiv x_H$, $z(t')\equiv 0$, and

$$u(t')=u(0)e^{-(\tau+\mu_2)t'}.$$

The y-compartment varies according to $dy/dt=\tau u(0)$ at time $t'=0$. If $u(0)\neq 0$, then $dy/dt>0$, implying that $y(t_0')\neq 0$ for some $t_0'\neq 0$; that is, the trajectory will leave the set I. For the solution $\omega(t')$ to remain in I for all t', we must have $u(0)=0$ and therefore $u(t')\equiv 0$. Subsequently, solving the initial value problem $dy/dt=0$, $y(0)=0$ yields $y(t')\equiv 0$. Taken all together, the above argument means that the maximal invariant set in I is comprised only of the single point $P_0=(x_H,0,0,0)$, i.e. $M=\{P_0\}$. □

A.4. Proof of Theorem 3.2. Part 3: stability of P^*

The final part of the proof of Theorem 3.2 is to demonstrate the global stability of the chronic infection equilibrium P^* whenever it exists in the Γ. We therefore establish the following.

Proposition A4 (*Global stability of P^**). *When $R_0>1$, the chronic-infection equilibrium P^* is globally asymptotically stable in $\mathring{\Gamma}$.*

Proof. Assume that $R_0>1$. Then by Proposition A1, the chronic infection equilibrium P^* exists in the feasible region Γ. To prove the result, we construct an appropriate Lyapunov function $V:\mathbb{R}^4_+\to\mathbb{R}$ that will allow us to conclude the global asymptotic stability of P^* in $\mathring{\Gamma}$.

Suppose that $(x(t),u(t),y(t),z(t))$ is a solution of model (1) and let

$$\begin{aligned}V&=\left(x-x^*-x^*\log\frac{x}{x^*}\right)+\left(u-u^*-u^*\log\frac{u}{u^*}\right)\\&\quad+\frac{\tau+\mu_2}{\tau}\left(y-y^*-y^*\log\frac{y}{y^*}\right)+\frac{\gamma}{\tau\nu}(\tau+\mu_2)z^*\left(z-z^*-z^*\log\frac{z}{z^*}\right).\end{aligned}$$

The function $V=V(x,u,y,z)$ is positive definite with respect to the chronic infection equilibrium point $P^*=(x^*,u^*,y^*,z^*)$. Taking the Lyapunov derivative along the solution $(x(t),u(t),y(t),z(t))$ yields

$$\begin{aligned}\frac{dV}{dt}&=\left(1-\frac{x^*}{x}\right)\frac{dx}{dt}+\left(1-\frac{u^*}{u}\right)\frac{du}{dt}+\frac{\tau+\mu_2}{\tau}\left(1-\frac{y^*}{y}\right)\frac{dy}{dt}\\&\quad+\frac{\gamma}{\tau\nu}(\tau+\mu_2)z^*\left(1-\frac{z^*}{z}\right)\frac{dz}{dt}\\&=\left(1-\frac{x^*}{x}\right)(\lambda-\beta xy-\mu_1x)+\left(1-\frac{u^*}{u}\right)(\beta xy+ry-(\tau+\mu_2)u)\\&\quad+\frac{\tau+\mu_2}{\tau}\left(1-\frac{y^*}{y}\right)(\tau u-\gamma yz-\mu_3y)\\&\quad+\frac{\gamma}{\tau\nu}(\tau+\mu_2)z^*\left(1-\frac{z^*}{z}\right)(\nu y-\mu_4z).\end{aligned}$$

By making the appropriate substitutions using the equilibrium equations (A.1a)–(A.1d), we find that

$$\begin{aligned}\frac{dV}{dt}&=\left(1-\frac{x^*}{x}\right)(\mu_1x^*-\mu_1x)+\left(1-\frac{x^*}{x}\right)(\beta x^*y^*-\beta xy)\\&\quad+\left(1-\frac{u^*}{u}\right)\left(\beta xy+ry-(\beta x^*y^*+ry^*)\frac{u}{u^*}\right)\\&\quad+\frac{\beta x^*y^*+ry^*}{\tau u^*}\left(1-\frac{y^*}{y}\right)\left(\tau u-\tau u^*\frac{y}{y^*}\right)\\&\quad+\frac{\tau+\mu_2}{\tau}\left(1-\frac{y^*}{y}\right)(\gamma yz^*-\gamma yz)\\&\quad+\frac{\gamma}{\tau\nu}(\tau+\mu_2)z^*\left(1-\frac{z^*}{z}\right)\left(\nu y-\nu y^*\frac{z}{z^*}\right)\\&=\mu_1x^*\left(2-\frac{x^*}{x}-\frac{x}{x^*}\right)+\beta x^*y^*\left(3-\frac{x^*}{x}-\frac{x}{x^*}\frac{u^*}{u}\frac{y}{y^*}-\frac{u}{u^*}\frac{y^*}{y}\right)\\&\quad+ry^*\left(2-\frac{u^*}{u}\frac{y}{y^*}-\frac{u}{u^*}\frac{y^*}{y}\right)+\frac{\gamma}{\tau}(\tau+\mu_2)yz^*\left(2-\frac{z}{z^*}-\frac{z^*}{z}\right)\le 0.\end{aligned}$$

The final line follows from the inequalities $\sqrt{a_1a_2}\le(a_1+a_2)/2$ and $\sqrt[3]{a_1a_2a_3}\le(a_1+a_2+a_3)/3$, where $a_1,a_2,a_3>0$; that is, the geometric mean of n positive numbers can be no greater than their arithmetic mean. Hence, the global stability of P^* has been established when $R_0>1$. □

A.5. Proof of Theorem 5.1

Consider the proviral load at equilibrium, $v^*=(u^*+y^*)/(x^*+u^*+y^*)$. From Eq. (A.2), we have

$$u^*+y^*=\frac{\mu_4}{\tau\nu}(\gamma z^*+\tau+\mu_3)z^*\quad\text{and}\quad x^*=\frac{\lambda\nu}{\beta\mu_4z^*+\nu\mu_1}.$$

To show the first part of the theorem, we compute

$$\frac{d}{dz^*}(u^*+y^*) = \frac{\mu_4}{\tau\nu}(2\gamma z^*+\tau+\mu_3) > 0,$$

and

$$\frac{dx^*}{dz^*} = -\frac{\beta\lambda\nu\mu_4}{(\beta\mu_4 z^*+\nu\mu_1)^2} < 0.$$

Then,

$$\begin{aligned}\frac{dv^*}{dz^*} &= \frac{d}{dz^*}\left(\frac{u^*+y^*}{x^*+u^*+y^*}\right)\\ &= \frac{(x^*+u^*+y^*)\frac{d}{dz^*}(u^*+y^*)-(u^*+y^*)\frac{d}{dz^*}(x^*+u^*+y^*)}{(x^*+u^*+y^*)^2}\\ &= \frac{1}{(x^*+u^*+y^*)^2}\left(x^*\frac{d}{dz^*}(u^*+y^*)-(u^*+y^*)\frac{dx^*}{dz^*}\right)\\ &= \frac{\mu_4}{\tau\nu(x^*+u^*+y^*)^2}\left[(2\gamma z^*+\tau+\mu_3)x^*+\frac{\beta\lambda\tau\nu^2(u^*+y^*)}{(\beta\mu_4 z^*+\nu\mu_1)^2}\right]\\ &> 0.\end{aligned}$$

Hence, the proviral load at equilibrium, v^*, is an increasing function of z^*.

The second part of the theorem is proved by observing that

$$\frac{dv^*}{d\gamma} = \frac{dv^*}{dz^*}\frac{dz^*}{d\gamma}.$$

It can be straight-forwardly shown that $dz^*/d\gamma < 0$, whose derivation follows directly from differentiating the equation $F(z^*) = 0$, where $F(z)$ is defined in Eq. (A.3), implicitly with respect to the parameter γ. Combined with the result from the first part of the theorem demonstrating that $dv^*/dz^* > 0$, we therefore conclude that

$$\frac{dv^*}{d\gamma} < 0;$$

that is, v^* is a decreasing function of γ.

Appendix B. Additional figures

See Figs. B1–B3.

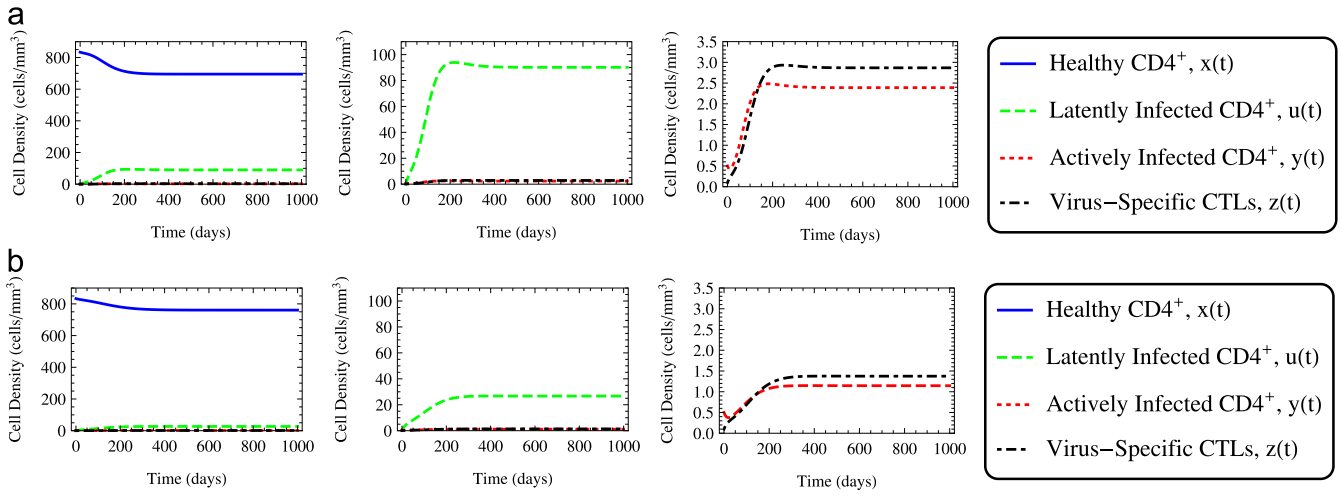

Fig. B1. Time series plots for each of the T-cell populations under investigation comparing exponential and logistic growth terms for infected target cell proliferation. (For interpretation of the references to colour in this figure caption, the reader is referred to the web version of this paper.). For the latter case, the carrying capacity k has been selected so that $x+u+y$ is of the order k. Specifically, $k=800$ cells/mm^3. Because the rate r of infected target cell proliferation differentially influences each of the two models, we therefore explored its impact on the various cell populations. We found that when the value of r was chosen in the physiologically relevant range as in Table 1, the two models converged to equilibria that were close to each other. In Figs. B1 and B2, we plotted the time evolution graphs with a value of r that is two orders of magnitude higher than in Table 1. We observe, as expected, that although the effect of a logistic growth term serves to control the magnitude of the infected cell populations and hence the proviral load, there is no qualitative difference in dynamical behaviour. All other parameters have been chosen as in Table 1 and are the same between the two models. (a) Model with exponential growth term (large r) and (b) model with logistic growth term (large r).

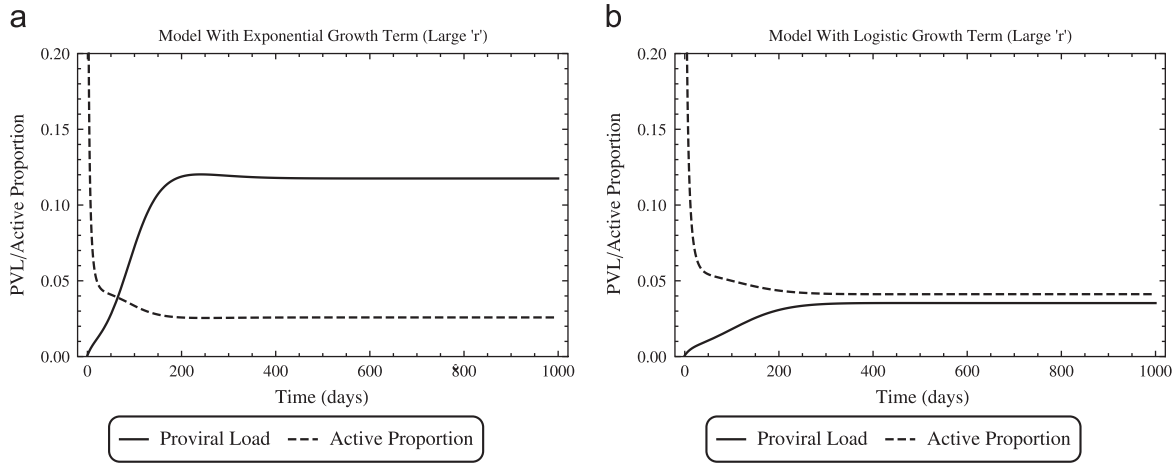

Fig. B2. Time series graphs for the proviral load and active proportion of infected cells comparing exponential and logistic growth terms for infected target cell proliferation.

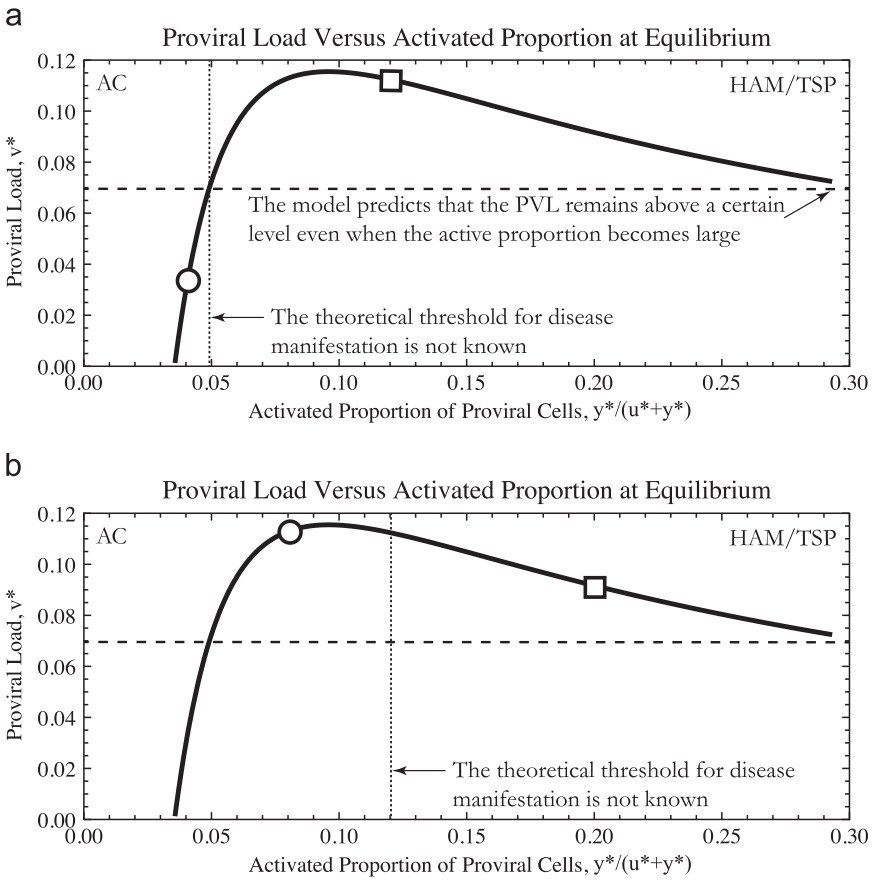

Fig. B3. Bifurcation diagram relating proviral load v^* and the active proportion of infected cells $y^*/(u^*+y^*)$. The results of our model are consistent with experimental and clinical observations, and can even account for some of the peculiarities of HTLV-I infection. In particular, it is known that although the magnitude of the proviral load of an HTLV-I seropositive individual is correlated with the presence of disease, there exists a broad overlap in the magnitudes of the proviral loads among ACs and HAM/TSP patients, and a high proviral load is neither necessary nor sufficient for the progression of HTLV-I-associated disease. Here, the rate γ of CTL-mediated lysis is fixed. The thin, dotted vertical line representing the theoretical threshold for disease manifestation corresponds to the thin, dotted horizontal line in Fig. 8(a). The precise position of this theoretical threshold is unknown. (a) If the threshold for disease manifestation is sufficiently low, then the proviral load of an AC (along the curve to the left of the threshold, for example, at the position of the open circle) would always be lower than that of a HAM/TSP patient (along the curve to the right of the threshold, for example, at the position of the open square). This represents the typical case whereby a HAM/TSP patient harbours a higher proviral load than that of an AC. (b) However, if the threshold for disease manifestation is sufficiently high, then our model demonstrates the theoretical possibility for the proviral load of an AC (along the curve to the left of the threshold, for example, symbolised by an open circle) to be above that of a HAM/TSP patient (along the curve to the right of the threshold, for example, symbolised by an open square).

References

Asquith, B., Bangham, C.R.M., 2000. The role of cytotoxic T lymphocytes in human T-cell lymphotropic virus type 1 infection. J. Theor. Biol. 207, 65–79.

Asquith, B., Bangham, C.R.M., 2007. Quantifying HTLV-I dynamics. Immunol. Cell Biol. 85, 280–286.

Asquith, B., Hanon, E., Taylor, G.P., Bangham, C.R.M., 2000. Is human T-cell lymphotropic virus type I really silent? Philos. Trans. R. Soc. B. 355, 1013–1019.

Asquith, B., Mosley, A.J., Barfield, A., Marshall, S.E.F., Heaps, A., Goon, P., Hanon, E., Tanaka, Y., Taylor, G., Bangham, C.R.M., 2005. A functional $CD8^+$ cell assay reveals individual variation in $CD8^+$ cell antiviral efficacy and explains differences in human T-lymphotropic virus type 1 proviral load. J. Gen. Virol. 86, 1515–1523.

Asquith, B., Bangham, C.R.M., 2008. How does HTLV-I persist despite a strong cell-mediated immune response? Trends Immunol. 29, 4–11.

Asquith, B., Mosley, A.J., Heaps, A., Tanaka, Y., Taylor, G., McLean, A.R., Bangham, C.R.M., 2005. Quantification of the virus-host interaction in human T lymphotropic virus type I infection. Retrovirology 2, 75–83.

Asquith, B., Zhang, Y., Mosley, A.J., de Lara, C.M., Wallace, D.L., Worth, A., Kaftantzi, L., Meekings, K., Griffin, G.E., Tanaka, Y., Tough, D.F., Beverly, P.C., Taylor, G.P., Macallan, D., Bangham, C.R.M., 2007. In vivo T lymphocyte dynamics in humans and the impact of human T-lymphotropic virus 1 infection. Proc. Natl. Acad. Sci. 104, 8035–8040.

Bangham, C.R.M., 2000. HTLV-1 infections. J. Clin. Pathol. 53, 581–586.

Bangham, C.R.M., 2009. CTL quality and the control of human retroviral infections. Eur. J. Immunol. 39, 1700–1712.

Bangham, C.R.M., Meekings, K., Toulza, F., Nejmeddine, M., Majorovits, E., Asquith, B., Taylor, G., 2009. The immune control of HTLV-I infection: selection forces and dynamics. Front. Biosci. 14, 2889–2903.

Bangham, C.R.M., 2003. The immune control and cell-to-cell spread of human T-lymphotropic virus type 1. J. Gen. Virol. 84, 3177–3189.

Bangham, C.R.M., Hall, S.E., Jeffery, K.J.M., Vine, A.M., Witkover, A., Nowak, M.A., Wodarz, D., Usuku, K., Osame, M., 1999. Genetic control and dynamics of the cellular immune response to the human T-cell leukaemia virus, HTLV-I. Philos. Trans. R. Soc. B. 354, 691–700.

Bangham, C.R.M., Osame, M., 2005. Cellular immune response to HTLV-1. Oncogene 24, 6035–6046.

Biddison, W.E., Kubota, R., Kawanishi, T., Taub, D.D., Cruikshank, W.W., Center, D.M., Connor, E.W., Utz, U., Jacobson, S., 1997. Human T cell leukemia virus type I (HTLV-I)-specific CD8+ CTL clones from patients with HTLV-I-associated neurologic disease secrete proinflammatory cytokines and matrix metalloproteinase. J. Immunol. 159, 2018–2025.

Bofill, M., Janossy, G., Lee, C.A., MacDonald-Burns, D., Phillips, A.N., Sabin, C., Timms, A., Johnson, M.A., Kernoff, P.B.A., 1992. Laboratory control values for CD4 and CD8 T lymphocytes. Implications for HIV-1 diagnosis. Clin. Exp. Immunol. 88, 243–252.

Gallo, R.C., 2005. The discovery of the first human retrovirus: HTLV-1 and HTLV-2. Retrovirology 2, 17–23.

Gaudray, G., Gachon, F., Basbous, J., Biard-Piechaczyk, M., Devaux, C., Mesnard, J.-M., 2002. The complementary strand of the human T-cell leukemia virus type 1 RNA genome encodes a bZIP transcription factor That down-regulates viral transcription. J. Virol. 76, 12813–12822.

Gillet, N.A., Malani, N., Melamed, A., Gormley, N., Carter, R., Bentley, D., Berry, C., Bushman, F.D., Taylor, G.P., Bangham, C.R.M., 2011. The host genomic environment of the provirus determines the abundance of HTLV-1-infected T-cell clones. Blood 117, 3113–3122.

Gómez-Acevedo, H., Li, M.Y., 2005. Backward bifurcation in a model for HTLV-I infection of $CD4^+$ T cells. Bull. Math. Biol. 67, 101–114.

Gómez-Acevedo, H., Li, M.Y., Jacobson, S., 2010. Multistability in a model for CTL response to HTLV-I infection and its implications to HAM/TSP development and prevention. Bull. Math. Biol. 72, 681–696.
Gonçalves, D.U., Proietti, F.A., Ribas, J.G.R., Araújo, M.G., Pinheiro, S.R., Guedes, A.C., Carneiro-Proietti, A.B.F., 2010. Epidemiology, treatment, and prevention of human T-cell leukemia virus type 1-associated diseases. Clin. Microbiol. Rev. 23, 577–589.
Goon, P.K.C., Biancardi, A., Fast, N., Igakura, T., Hanon, E., Mosley, A.J., Asquith, B., Gould, K.G., Marshall, S., Taylor, G.P., Bangham, C.R.M., 2004. Human T cell lymphotropic virus (HTLV) type-1-specific $CD8^+$ T cells: frequency and immunodominance hierarchy. J. Infect. Dis. 189, 2294–2298.
Höllsberg, P., 1999. Mechanisms of T-Cell activation by human T-cell lymphotropic virus type I. Microbiol. Mol. Biol. Rev. 63, 308–333.
Igakura, T., Stinchcombe, J.C., Goon, P.K.C., Taylor, G.P., Weber, J.N., Griffiths, G.M., Tanaka, Y., Osame, M., Bangham, C.R.M., 2003. Spread of HTLV-I between lymphocytes by virus-induced polarization of the cytoskeleton. Science 299, 1713–1716.
Jeffery, K.J.M., Usuku, K., Hall, S.E., Matsumoto, W., Taylor, G.P., Procter, J., Bunce, M., Ogg, G.S., Welsh, K.I., Weber, J.N., Lloyd, A.L., Nowak, M.A., Nagai, M., Kodama, D., Izumo, S., Osame, M., Bangham, C.R.M., 1999. HLA alleles determine human T-lymphotropic virus-I (HTLV-I) proviral load and the risk of HTLV-I-associated myelopathy. Proc. Natl. Acad. Sci. USA 96, 3848–3853.
Kalajdzievska, D., Li, M.Y., 2011. Modeling the effects of carriers on transmission dynamics of infectious diseases. Math. Biosci. Eng. 8, 711–722.
Kirschner, D., Webb, G.F., 1996. A model for treatment strategy in the chemotherapy of AIDS. Bull. Math. Bio. 58, 367–390.
Korobeinikov, A., Wake, G.C., 2002. Lyapunov functions and global stability for SIR, SIRS, and SIS epidemiological models. Appl. Math. Lett. 15, 955–960.
Korobeinikov, A., 2004. Global properties of basic virus dynamics models. Bull. Math. Biol. 66, 879–883.
Kubota, R., Kawanishi, T., Matsubara, H., Manns, A., Jacobson, S., 2000. HTLV-I specific IFN-$\gamma+$ CD8+ lymphocytes correlate with the proviral load in peripheral blood of infected individuals. J. Neuroimmunol. 102.
Kubota, R., Hanada, K., Furukawa, Y., Arimura, K., Osame, M., Gojobori, T., Izumo, S., 2007. Genetic stability of human T lymphotropic virus type I despite antiviral pressures by CTLs. J. Immunol. 178, 5966–5972.
LaSalle, J.P., 1976. The Stability of Dynamical Systems, CBMS-NSF Regional Conference Series in Applied Mathematics. SIAM, Philadelphia.
Li, M.Y., Lim, A.G., 2011. Modelling the role of Tax expression in HTLV-I persistence in vivo. Bull. Math. Biol. 73, 3008–3029.
Matsuoka, M., Green, P.L., 2009. The HBZ gene, a key player in HTLV-I pathogenesis. Retrovirology 6, 71.
Meekings, K.N., Leipzig, J., Bushman, F.D., Taylor, G.P., Bangham, C.R.M., 2008. HTLV-I integration into transcriptionally active genomic regions is associated with proviral expression and with HAM/TSP. PLoS Pathog. 4, e1000027.
Melamed, A., Laydon, D.J., Gillet, N.A., Tanaka, Y., Taylor, G.P., Bangham, C.R.M., 2013. Genome-wide determinants of proviral targeting, clonal abundance and expression in natural HTLV-1 infection. PLoS Pathog. 9, e1003271.
Mortreux, F., Gabet, A.S., Wattel, E., 2003. Molecular and cellular aspects of HTLV-I associated leukemogenesis in vivo. Leukemia 17, 26–38.
Mosley, A.J., Asquith, B., Bangham, C.R.M., 2005. Cell-mediated immune response to human T-lymphotropic virus type I. Viral Immunol. 18, 293–305.
Mosley, A.J., Bangham, C.R.M., 2009. A new hypothesis for the pathogenesis of Human T-lymphotropic virus type 1 associated myelopathy/tropical spastic paraparesis. Biosci. Hypotheses 2, 118–124.
Nagai, M., Kubota, R., Greten, T.F., Schneck, J.P., Leist, T.P., Jacobson, S., 2001. Increased activated human T cell lymphotropic virus type I HTLV-I Tax11-19-specific memory and effector CD8+ cells in patients with (HTLV-I)-associated myelopathy/tropical spastic paraparesis: correlation with HTLV-I provirus load. J. Infect. Dis. 183, 197–205.
Nelson, P.W., Murray, J.D., Perelson, A.S., 2000. A model of HIV-1 pathogenesis that includes an intracellular delay. Math. Biosci. 163, 201–215.
Nowak, M.A., Bangham, C.R.M., 1996. Population dynamics of immune responses to persistent viruses. Science 272, 74–79.
Parham, P., 2005. The Immune System, Garland Science, New York.
Parker, C.E., Daenke, S., Nightingale, S., Bangham, C.R.M., 1994. Activated, HTLV-1-specific cytotoxic T-lymphocytes are found in healthy seropositives as well as in patients with tropical spastic paraparesis. Virology 188, 628–636.
Perelson, A.S., 1989. Modeling the interaction of the immune system with HIV. In: Castillo-Chavez, C. (Ed.), Mathematical and Statistical Approaches to AIDS Epidemiology. Lecture Notes in Biomathematics, vol. 83. Springer, Berlin, pp. 350–370.
Proietti, F.A., Carneiro-Proietti, A.B.F., Catalan-Soares, B.C., Murphy, E.L., 2005. Global epidemiology of HTLV-I infection and associated diseases. Oncogene 24, 6058–6068.
Ribeiro, R.M., Mohri, H., Ho, D.D., Perelson, A.S., 2002. In vivo dynamics of T cell activation, proliferation, and death in HIV-1 infection: why are $CD4^+$ but not $CD8^+$ T cells depleted?. Proc. Natl. Acad. Sci. 99, 15572–15577.
Richardson, J.H., Höllsberg, P., Windhagen, A., Child, L.A., Lever, A.M.L., 1997. Variable immortalizing potential and frequent virus latency in blood-derived T-cell clones infected with human T-cell leukemia virus type I. Blood 89, 3303–3314.
Shiraki, H., Sagara, Y., Inoue, Y., 2003. Cell-to-cell transmission of HTLV-I. In: Two Decades of Adult T-cell Leukemia and HTLV-I Research, Gann Monograph on Cancer Research, No. 50, Japan Scientific Societies Press, Tokyo, pp. 303–316.
Wodarz, D., Hall, S.E., Usuku, K., Osame, M., Ogg, G.S., McMichael, A.J., Nowak, M.A., Bangham, C.R.M., 2001. Cytotoxic T-cell abundance and virus load in human immunodeficiency virus type 1 and human T-cell leukaemia virus type 1. Proc. R. Soc. Lond. B.: Biol. Sci. 268, 1215–1221.